

ALMA MATER STUDIORUM - UNIVERSITY OF BOLOGNA

---

SCHOOL OF ENGINEERING AND ARCHITECTURE

*CASY Center for Research on Complex Automated Systems*

*DEI Department of Electrical, Electronic, and Information Engineering "Guglielmo Marconi"*

MASTER DEGREE IN AUTOMATION ENGINEERING

GRADUATION THESIS

in

System Theory and Advanced Control

**AUTOMATIC SEARCH OF MISSING PEOPLE IN  
AVALANCHES**

CANDIDATE

**Francesco Ricciardi**

SUPERVISOR

**Eminent Prof.  
Lorenzo Marconi**

CO-SUPERVISOR

**Dott. Nicola Mimmo**

Academic Year 2016/2017

Graduation Session III



# Abstract

One of the main source of danger for people practising activities in mountain environments is avalanches. In the early 70s has been commercialized the first model of avalanche beacon transceiver: a device, composed by a transmitter and a receiver, specialized to the purpose of finding people buried under the snow. Since 2013, project SHERPA is working to develop ground and aerial robots to support human in the search of missing people in avalanches.

The aim of this dissertation is to provide a way to interface an avalanche beacon receiver (ARTVA) with the autopilot module mounted on a quad-copter drone, and to study and realize a software implementation of two automatic search algorithms, with the intention of speeding up search operations with drones.

First we will focus on interfacing the ARTVA system with a quad-copter autopilot module, named Pixhawk. This module embed a software, named PX4, which runs on a real-time operating system (RTOS), and have several connection ports, among which there is the serial one that we will use for our purpose. Then we will analyse how to use the data coming from the ARTVA receiver to construct and implement the two search algorithms. The idea is to generate set-points, based on the information coming from the avalanche beacon receiver, and use them to feed the position controller which is implemented in the PX4 firmware. Finally, we will execute simulations, provide results, and investigate if a practical implementation is possible and what are the relative issues.

*Le valanghe sono una delle principali fonti di pericolo per coloro che praticano attività in montagna. All'inizio degli anni '70 è stato commercializzato il primo modello di apparecchio di ricerca travolti in valanga: si tratta di un dispositivo, composto da un trasmettitore e un ricevitore, specializzato per la ricerca di persone seppellite nella neve. Fin dal 2013,*

*il progetto SHERPA sta lavorando allo sviluppo di un sistema di robot terrestri e aerei con lo scopo di supportare l'uomo nella ricerca di dispersi in valanga.*

*L'obiettivo di questa trattazione è quello di trovare un modo per interfacciare il sistema di ricerca dispersi in valanga con il modulo autopilota montato su un drone quadricottero, e di studiare e realizzare una implementazione software di due algoritmi di ricerca automatica, così da poter velocizzare le operazioni di ricerca con i droni.*

*In primis verrà realizzato l'interfacciamento tra il sistema ARTVA e Pixhawk, un modulo autopilota per quadricotteri. Il suddetto modulo incorpora un software, chiamato PX4, che esegue su un sistema operativo in tempo reale, e inoltre dispone di diversi connettori, tra cui la porta seriale che verrà utilizzata al nostro scopo. Poi si indagherà come utilizzare i dati ricevuti da ARTVA per costruire e utilizzare i due algoritmi di ricerca. L'idea è quella di generare dei riferimenti, basandosi sui dati ottenuti dal ricevitore, e di mandarli al controllore di posizione già implementato nel firmware di PX4. Infine, verranno eseguite delle simulazioni, verranno mostrati i risultati, e si cercherà di capire se è possibile una implementazione pratica e quali sono i relativi problemi.*

# Contents

<b>Abstract</b>	<b>3</b>
<b>1 Introduction</b>	<b>15</b>
1.1 Motivations . . . . .	15
1.2 State of the art . . . . .	16
<b>2 ARTVA system and search algorithms</b>	<b>19</b>
2.1 ARTVA system interfacing . . . . .	19
2.1.1 ARTVA protocol data block . . . . .	21
2.1.2 Reading ARTVA data . . . . .	23
2.1.3 Data validation algorithm . . . . .	27
2.2 Flux Line search technique . . . . .	29
2.2.1 Mathematical description . . . . .	30
2.2.2 Implementation . . . . .	33
2.3 Extremum Seeking search technique . . . . .	35
2.3.1 SISO scheme and linear analysis . . . . .	35
2.3.2 Non-local stability of non-linear case . . . . .	38
2.3.3 Hybrid Extremum Seeking Control . . . . .	43
2.3.4 Implementation . . . . .	47
2.4 General control scheme . . . . .	49
<b>3 Results</b>	<b>51</b>
3.1 Simulations . . . . .	51
3.1.1 Flux Line algorithm simulation . . . . .	53
3.1.2 HESC algorithm simulation . . . . .	56

3.1.3	Algorithms comparison . . . . .	60
3.2	Practical implementation . . . . .	61
3.2.1	Test with motors off . . . . .	61
3.2.2	Test with motors on and no shielding . . . . .	62
3.2.3	Test with motors on and standard aluminium shielding . . . . .	63
3.2.4	Test with motors on and EMI aluminium shielding . . . . .	64
<b>Conclusions</b>		<b>65</b>
<b>A First Appendix</b>		<b>67</b>
A.1	PX4 . . . . .	67
A.1.1	Flight stack . . . . .	67
A.1.2	Middleware . . . . .	68
A.1.3	NuttX . . . . .	68
A.2	Communication over serial port . . . . .	68
A.2.1	Asynchronous serial protocol . . . . .	69
A.2.2	Rules of serial communication . . . . .	70
A.3	Publish/subscribe structure . . . . .	71
A.3.1	Adding a new topic . . . . .	72
A.3.2	Publish into a topic . . . . .	72
A.3.3	Subscribe to a topic . . . . .	73
A.4	ROS . . . . .	74
A.4.1	Creating a package . . . . .	74
A.4.2	Building the workspace and sourcing the setup file . . . . .	74
A.4.3	ROS nodes . . . . .	75
A.4.4	ROS topics . . . . .	75
A.4.5	Launch a ROS node with a launch file . . . . .	75
<b>B Second Appendix</b>		<b>77</b>
B.1	ARTVA system interfacing . . . . .	77
B.1.1	Reading ARTVA data . . . . .	77
B.1.2	Data validation algorithm . . . . .	80

---

B.2 Algorithms implementation . . . . .	84
B.2.1 Flux Line algorithm . . . . .	84
B.2.2 HESC algorithm . . . . .	86
<b>Bibliography</b>	<b>89</b>





# List of Figures

1.1	Grid and Cross Flight algorithms operation . . . . .	17
2.1	Magnetic dipole: moment and magnetic field . . . . .	20
2.2	Data validation algorithm flowchart . . . . .	28
2.3	Flux Line search technique operation . . . . .	30
2.4	Extremum Seeking Control scheme for a static map . . . . .	35
2.5	Extremum Seeking Control scheme for plants with dynamics . . . . .	37
2.6	First order Extremum Seeking control scheme . . . . .	40
2.7	Higher order Extremum Seeking control scheme . . . . .	42
2.8	General control scheme . . . . .	50
3.1	Flux Line algorithm simulation case A . . . . .	54
3.2	Flux Line algorithm simulation case B . . . . .	54
3.3	Flux Line algorithm simulation case C . . . . .	55
3.4	Flux Line algorithm simulation case D . . . . .	55
3.5	Circle-shaped HESC algorithm simulation case A . . . . .	56
3.6	Circle-shaped HESC algorithm simulation case B . . . . .	57
3.7	Circle-shaped HESC algorithm simulation case C . . . . .	57
3.8	Circle-shaped HESC algorithm simulation case D . . . . .	58
3.9	Eight-shaped HESC algorithm simulation case A . . . . .	58
3.10	Eight-shaped HESC algorithm simulation case B . . . . .	59
3.11	Eight-shaped HESC algorithm simulation case C . . . . .	59
3.12	Eight-shaped HESC algorithm simulation case D . . . . .	60
A.1	Flight stack architecture . . . . .	68

A.2	Example of parallel interface . . . . .	69
A.3	Example of serial interface . . . . .	69
A.4	Example of a serial data frame . . . . .	71

# List of Tables

2.1	Protocol data block . . . . .	22
3.1	Algorithms comparison . . . . .	61
3.2	Test results: motors off . . . . .	62
3.3	Test results: motors on, no shielding . . . . .	63
3.4	Test results: motors on, simple aluminium shielding . . . . .	63
3.5	Test results: motors on, EMI aluminium shielding . . . . .	64



# List of Achronyms

<b>SHERPA</b>	Smart collaboration between Humans and ground-aerial Robots for improving rescuing activities in Alpine environment
<b>ARTVA</b>	<i>Apparecchio di Ricerca Travolti in Valanga</i> , search device of people overwhelmed in avalanches
<b>RTOS</b>	Real-Time Operating System
<b>ICAR</b>	International Commission for Alpine Rescue
<b>GPS</b>	Global Positioning System
<b>CRC</b>	Cyclic Redundancy Check
<b>SISO</b>	Single-Input Single-Output
<b>SPA</b>	Semi-global Practical Asymptotically
<b>HESC</b>	Hybrid Extremum Seeking Control
<b>FIFO</b>	First In First Out
<b>ROS</b>	Robot Operating System
<b>ESC</b>	Electronic Speed Controller
<b>EMI</b>	Electromagnetic Interference
<b>API</b>	Application Programming Interface



# Chapter 1

## Introduction

The goal of this project was to study, realize and simulate automatic search algorithms with the aim of implementing them on a quad-copter drone by means of an autopilot module. The aforesaid algorithms have the purpose to guide the drone toward people buried under the snow in avalanches, so to minimize the time spent on the search, and ensure a prompt intervention from rescuers. Those algorithms are generated using data coming from an avalanche beacon system (ARTVA).

Since February 1st 2013 the European project SHERPA[1] is involved in the development of a mixed ground and aerial robotics platform to support human in search and rescue activities in unfriendly and hostile environments, like the alpine rescuing scenario, which is specifically targeted by the project.

### 1.1 Motivations

A research made by the International Commission for Alpine Rescue (ICAR)[2] shows that about 150 people are killed by avalanches every year in Europe and North America. The overall survival rate of avalanche victims is 77%, and it mainly depends on the grade and duration of burial. The analysis of a Swiss sample showed that 39% of people involved in an avalanche were completely buried, and the survival probability in those cases is 47.6%, versus 95.8% in cases of partial burial. These data highlight that grade of burial is the strongest single factor for survival.

The above mentioned analysis shows also that survival probability remains above 80%

until 18 minutes after burial, a lapse of time referred as survival phase, falling thereafter to 32%, in the so-called asphyxia phase. Another noticeable decrease in survival occurs after 90 minutes, due to hypothermia combined with hypoxia and hypercapnia. Therefore, also the duration of burial is very important and has to be taken in consideration. Asphyxia was found to be the most common cause of death, and may occur in combination with trauma and hypothermia. So, the main recommendation is to locate and extricate buried victims as quick possible.

The objective of SHERPA is to use quad-copters, which are not slowed by the hostility of the terrain, to perform an automatic and rapid search of the victim, in such a way to speed up the human intervention.

## 1.2 State of the art

As far as now, the efficiency of quad-copter drones supported by ARTVA systems in rescuing operations has been tested with the implementation of a two phases search algorithm, while a terrain following one is in charge of making the vehicle maintain always a certain altitude from the ground.

After take-off, the quad-copter reaches a defined altitude and starts the Grid Flight[3] phase, during which it follows previously defined length parallel lines, placed at a certain distance from each other. More precisely, the drone travels a line until its end, then it move toward the next line following a trajectory perpendicular to the lines, and, once reached the next line, it travels that line backward until the end, keeping on describing a sort of grid-shaped path until the first signal coming from the beacon is acquired.

At this point, the Cross Flight phase starts, making the quad-copter perform the following operations:

- Forward flight until the beacon signal is lost, storing the GPS position when it happens; then, the flight segment continues to ensure avoiding false null signal detection and, in the case, the GPS position is updated.
- Backward flight until the beacon signal is found again and continue flying until it is lost, storing so the second GPS point.



- The autopilot module computes the midpoint between the two GPS acquired location and lead the drone to it.
- Turn  $90^\circ$  and repeat the forward and backward flight in order to identify the next two GPS points, namely the other two vertices of the cross.
- The autopilot module computes the midpoint between the two GPS acquired location and flies the quad-copter to it.

This point should be the one with the highest signal strength corresponding to the position of the transmitting beacon. The operation of this algorithm is shown in Figure 1.1. This search algorithm has been found to perform well, especially when wide areas need to be surveyed. However, our purpose is to improve search times by replacing the Cross Flight phase with an algorithm that is capable of drive the vehicle directly to the position of the beacon transmitter.

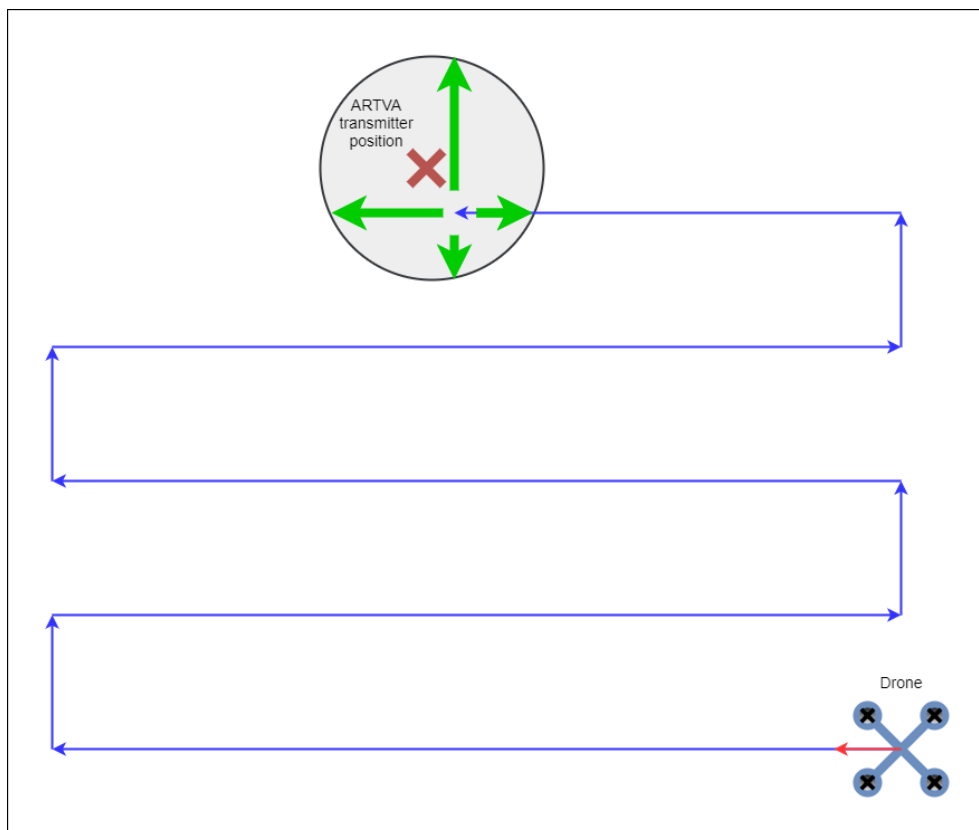


**Figure 1.1.** Grid and Cross Flight algorithms operation: the blue arrows represent Grid Flight, the green arrows represent Cross Flight, the red cross represents the transmitter's position.



# Chapter 2

## ARTVA system and search algorithms

Now we will analyse first the ARTVA beacon system and how to interface it to Pixhawk autopilot module, and so to read and handle the data coming from the ARTVA receiver with PX4 software running on the aforementioned module. Then we will study two possible search algorithms and how to implement them. The description of PX4 software and some of its basic concept are reported in the first appendix, while all the code used to realize the interfacing between the beacon receiver and the autopilot module, the reading of data, and the implementation of the search algorithms, is reported in the second appendix.

### 2.1 ARTVA system interfacing

The avalanche beacon system (ARTVA) used in our application includes a transmitter and a receiver which can be mounted on the quad-copter drone and activated during the search of missing people. Typical features of beacon transmitters are:

- carrier frequency of 457 kHz,
- up to 200 hours battery life,
- search range of about 50 metres.

ARTVA transmitter's flux lines behave as the external magnetic field produced by the magnetic dipole moment, represented in Figure 2.1; they propagate from a pole to the opposite one, following an ellipse fashion with growing amplitude. Conversely, the ARTVA receiver transform the signal received from the transmitter in two values:

**Distance ( $d$ )** Represents receiver's distance from the transmitter and it is computed as the inverse of signal's intensity.

**Angle ( $\delta$ )** It is the angle between the direction of the receiver and the line tangent to the flux ellipse to which the receiver is located.

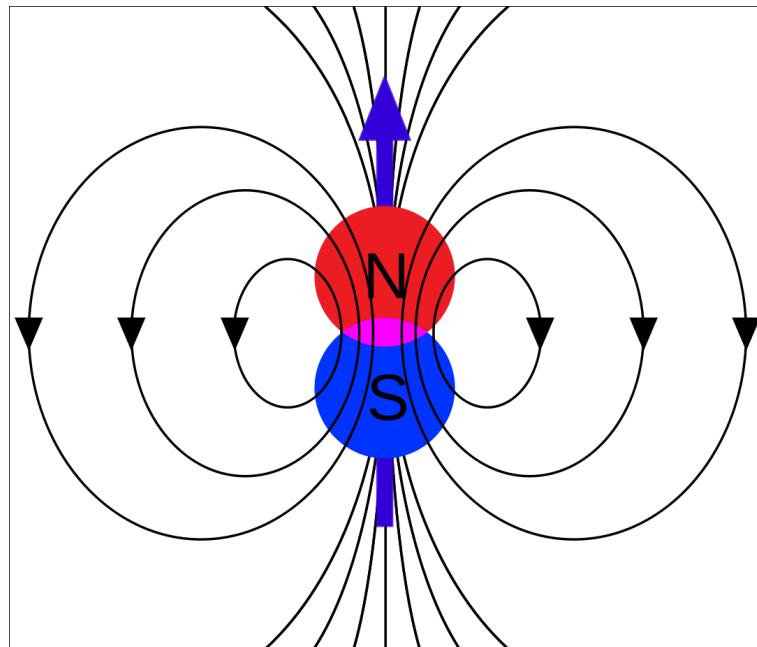


**Figure 2.1.** Magnetic dipole: the blue thick arrow represents the moment, the black thin arrows represent the magnetic field.

It is possible to identify three operation zones, depending on the distance between the transmitter and the receiver:

**Outer zone** The transmitter is too far from the receiver, the received distance value  $d$  is equal to  $-1$  or to the designed maximum value, depending on the model of the receiver, while the received angle value  $\delta$  is equal to zero.

**Mid zone** The receiver distance value  $d$  is in the range between 250 and the designed maximum value, while the received angle value  $\delta$  can vary between  $-90$  and  $+90$ ,

which are intended to be degrees, depending on the orientation of the receiver with respect to the transmitter.

**Inner zone** The transmitter is close to the receiver (in a radius of about 3 metres), the received distance value  $d$  is lower or equal to 300, while the received angle value  $\delta$  is equal to zero.

The middle and the inner zones are the useful ones, providing information about the transmitter's position, while we cannot conclude anything with the data obtained in the outer zone, except that we are too far from the target.

### 2.1.1 ARTVA protocol data block

The message sent from the ARTVA receiver to Pixhawk autopilot module is a 32 byte length data block, with 8-N-1 data format, sent with a baud rate of 9600 bps. The frequency of transmission is 5 Hz, so a new message is sent each 200 ms. Moreover, the number format of the message is little-endian.

The structure of the data block is presented in Table 2.1: as we can see, the first 4 bytes are reserved for the protocol header, bytes from 5 to 20 contains the useful data, byte 21 indicates the number of transmitter which is in focus, while byte 22 is an incremental counter. Then there are a bunch of bytes, from 23 to 27, which are unused, followed by a single byte which is used for the CRC-8 checksum. Finally, the last 4 bytes are reserved for the protocol footer.

**Protocol's header and footer** As said before, both the protocol's header and footer are 4 bytes length, and, as the names suggest, they are placed at the start and at the end of the data block, respectively. They are used in the validity check phase to distinguish between correct messages and broken ones. Both of them are a fixed hexadecimal number,  $0 \times BABEFADE$  for the header and  $0 \times EDAFEBAB$  for the footer, both expressed in little-endian number format.

**Useful data** The useful data of the messages are represented by 4 distances and 4 angles. The distance and angle values that we need depend on the number of transmitter in focus, e.g. if transmitter in focus is the number 1, we need to

Byte #	Description	Data format	Content range	Unit
1 - 4	Protocol start	unsigned int	$0 \times BABEFADE$	-
5 - 6	Distance to transmitter #1	unsigned short	0...65535	cm
7 - 8	Angle of transmitter #1 (most left ... most right)	signed short	-90... + 90	°
9 - 10	Distance to transmitter #2	unsigned short	0...65535	cm
11 - 12	Angle of transmitter #2 (most left ... most right)	signed short	-90... + 90	°
13 - 14	Distance to transmitter #3	unsigned short	0...65535	cm
15 - 16	Angle of transmitter #3 (most left ... most right)	signed short	-90... + 90	°
17 - 18	Distance to transmitter #4	unsigned short	0...65535	cm
19 - 20	Angle of transmitter #4 (most left ... most right)	signed short	-90... + 90	°
21	Transmitter # in focus (0: no transmitter already detected)	unsigned char	0...4	-
22	Data block counter (incremental / free running)	unsigned char	0...255	-
23	unused	unsigned char	$0 \times 00$	-
24	unused	unsigned char	$0 \times 00$	-
25	unused	unsigned char	$0 \times 00$	-
26	unused	unsigned char	$0 \times 00$	-
27	unused, reserved for CRC-16 Checksum	unsigned char	$0 \times 00$	-
28	CRC-8 Checksum from byte 5 to 26	unsigned char	0...255	-
29 - 32	Protocol end	unsigned int	$0 \times EDAFEBAB$	-

**Table 2.1.** Protocol data block.

acquire values from distance 1 and angle 1. The distance to transmitter value is a 2 bytes unsigned integer number in the range between 0 and 65535, and represents a distance in centimetres; the angle of transmitter value is a 2 bytes signed integer number in the range between  $-90$  and  $+90$ , and represents an angle in degrees. Each byte contains an hexadecimal number and, as said before, all values are expressed in little-endian number format, so we will need to use the techniques of masking and bit-shifting to reconstruct the values in such a way we can use them as decimal numbers.

**Scrambler** Another thing to take into account is that the data block is scrambled by adding the hexadecimal number  $0 \times 55$  to each byte, in such a way to avoid long sequences of 0 and 1. Thus, for descrambling data, we have to subtract  $0 \times 55$  from each byte.

**CRC-8 checksum** The checksum is used to verify data integrity, detecting error that may be introduced during the transmission. The CRC-8 checksum is a single byte unsigned character, which can assume integer values between 0 and 255, generated based on generator polynomial  $g(x) = x^8 + x^2 + x + 1$ .

### 2.1.2 Reading ARTVA data

The procedure used to read the data sent through the serial port by the ARTVA receiver is implemented in a Pixhawk module named *artva*, and is composed of the following steps:

- setting up and opening of the serial port (autopilot module side);
- read the arriving message;
- check the validity of the message;
- parse the message.

After these steps are correctly executed, the decoded message is ready to be published in the apposite topic. Basic concepts of communication over a serial port are reported in the first appendix. Now we will analyse each step of the reading procedure.

### Setup and open serial port

In this step, we first set up the port by specifying the *uart* name of the serial port to be opened, in our case */dev/ttyS6* (which corresponds to the serial 4 port of the Pixhawk), and the data format, which, as previously said, is 8-N-1 9600 bps baud rate. Then we can open the serial port by associating a file descriptor *fd* to the *open()* function as follows:

```
fd = open(port, O_RDONLY | O_NOCTTY | O_NDELAY);
```

Where *port* is the name of the serial port, and the other three terms in the second field of the function are flags. If the file descriptor *fd* returns a value equal or lower than 0, it means that the connection to the port is failed; otherwise, the setting up and opening procedure is finished and we can go on reading the message.

### Read the message

The *read()* function can read from a serial port only one byte for each call so, if we want to read a packet of bytes, we have to perform a call of the *read()* function for each byte. This means that in our case, in which we want to read a 32 byte data block, we have to realize a read cycle by means of a *while()* loop, so to execute a single *read()* for each byte. The reading algorithm is executed by calling the following function:

```
int read_port()
```

The *while()* loop does not start until the procedure reads a byte containing the hexadecimal number  $0 \times DE$ , which is the first byte of the message's header. This is a precaution needed to avoid the corruption of the data. In fact, it may happen that one or more bytes are skipped for any reason. If this happens, performing the read procedure by just using the *while()* loop will result in having a message buffer in which the header, the content and the footer are not in the right places, because each byte in the buffer has been shifted from its original position. This will lead to read all non-valid message, since now the first 4 bytes of the buffer do not contain the right values of the header (and the same is for the last 4 bytes which does not match the footer), and it will be the same for all the successive reading cycles.



By performing the read of the first byte out of the cycle, we can ensure that, even if there is a lose of some bytes, the reading cycle does not start until the algorithm recognizes the header's first byte, and so the positions of the next message's bytes are not shifted. Moreover, the buffer is cleaned at each new message read procedure, and the data are descrambled by subtracting the hexadecimal number  $0 \times 55$  to each byte.

### Validity check

The check of the message validity is performed by just ensuring that the values of the first 4 bytes and of the last 4 ones are equal to the values of the header and the footer. To run the validity check algorithm, we have to call the following function:

```
int check_ARTVA()
```

If a message does not pass the validity check, it is discarded and the algorithm wait for the next message.

### Message parsing

This part of the reading procedure has the purpose of reorder the bytes which constitute the useful part of the message, namely distances and angles values, so to transform the number format from little-endian to big-endian. The techniques of masking and bit-shifting, used for this transformation, can be summarized in the following steps:

- take the 2 bytes we want to transform (e.g. 00000010 00101001 in binary) and take, as a mask, the hexadecimal number  $0 \times FF00$ , which corresponds to the binary number 11111111 00000000, then perform an *AND* operation:

$$0000010\ 00101001\ \text{AND}\ 11111111\ 00000000 = 00000010\ 00000000$$

- Shifting the first of the 2 so obtained bytes to the right 8 places, we have basically found the first byte:

$$00000000\ 0000010$$

- Repeating now the same *AND* operation, but taking a slightly different mask, namely the hexadecimal number  $0 \times 00FF$ , corresponding to the binary number 00000000 11111111:

$$00000010\ 00101001\ \text{AND}\ 00000000\ 11111111 = 00000000\ 00101001$$

- Shifting these 2 bytes to the left 8 places by using the  $\ll 8$  operator, we found the second byte:

$$00101001\ 00000000$$

- Finally, summing up the 2 obtained bytes, we found the 2 bytes reordered in big-endian number format:

$$00101001\ 00000010$$

To execute the message parsing, this function must be called:

```
int parse_ARTVA()
```

By means of the masking and bit-shifting techniques applied on the message sent by the ARTVA receiver, we are able to reconstruct the distances and the angles values expressed in decimal numbers.

### **Publishing data**

When the reading procedure is complete and the message has been correctly decoded, the values of distances and angles, the value representing the transmitter in focus, and the value of the data block counter are published into a topic named *artva\_data* so that they can be recalled and used in real-time by the Pixhawk module which performs the ARTVA data validation and the set-point generation. The string of code used to publish the data is the following:

```
orb_publish(ORB_ID(artva_data), artva_topic_pub, &sens);
```

The publish/subscribe structure and how to use it is described in the first appendix.

### 2.1.3 Data validation algorithm

Once a new ARTVA measure has been read, we need to check if it is a valid one, so to discard all eventual wrong values coming from disturbances and electromagnetic noises. In order to check the validity of a measure, we have to check if it is consistent with the last values found, namely if it does not differ too much from them. To perform this data validation, the PX4 module *set\_point*, which is in charge of computing the set-point values (position or velocity, depending on the algorithm in use) to feed the controller, contains also a two-phase validation procedure.

The first thing to do is subscribe to the topic containing the data we need: the topic containing the data read from ARTVA, and the one containing the vehicle position, since we will later need to know the yaw angle of the quad-copter. We can subscribe to those topics by means of the following strings of code:

```
orb_check(artva_topic_sub, &updated);
if (updated) orb_copy(ORB_ID(artva_data), artva_topic_sub, &sensor);
orb_check(yaw_topic_sub, &updated);
if (updated) orb_copy(ORB_ID(vehicle_local_position), yaw_topic_sub, &pos);
```

The *set\_point* module runs first a parse algorithm to determine which of the four pairs of values (distances and angles) are the interesting ones, then executes the following two functions:

- first validation,
- step validation,

which together constitute the data validation algorithm. A flowchart of the algorithm is shown in Figure 2.2.

#### Parsing data

The parsing function decides which distance and angle values to take in consideration by just selecting the distance value which is below the admissible threshold, imposed to 2500 (about 25 metres), and its relative angle value. If there are no distances values below the threshold, the function says that no transmitter has been detected. This function

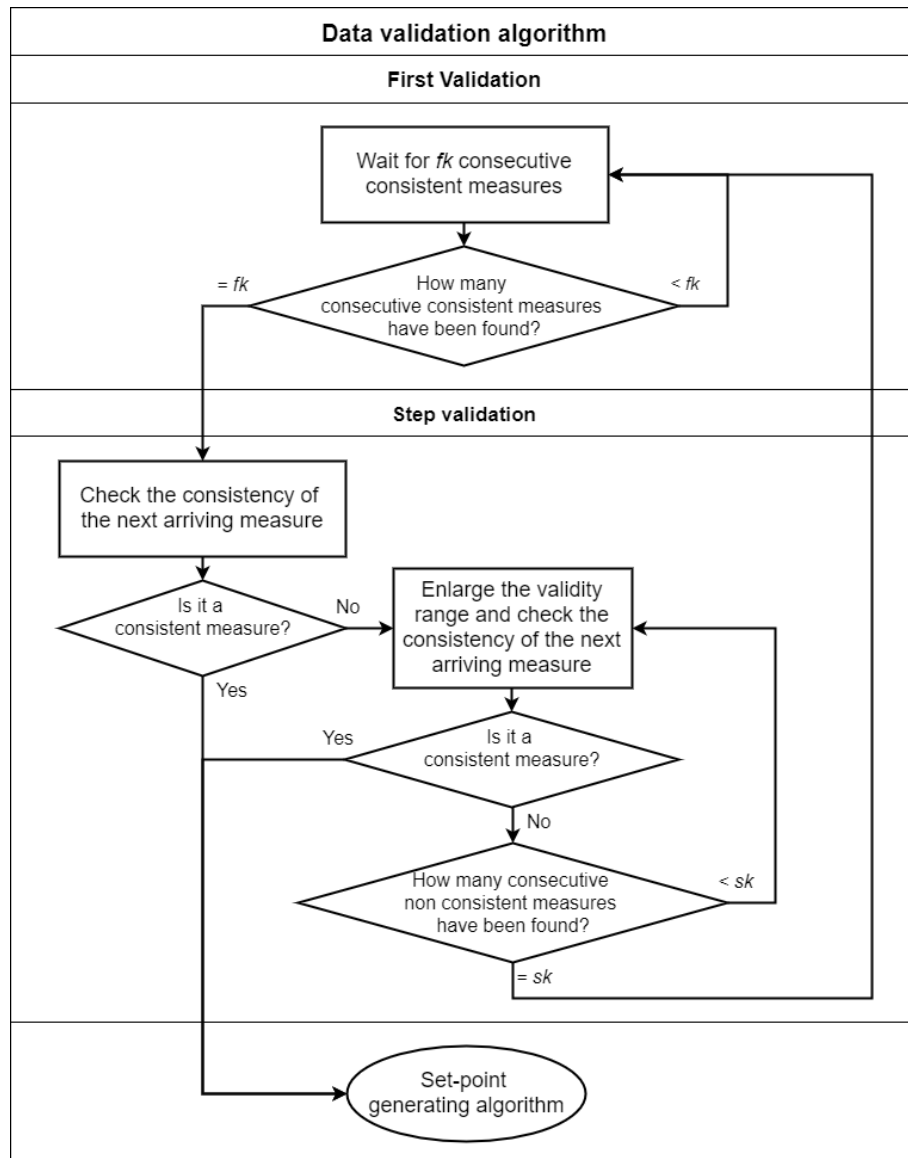


**Figure 2.2.** Data validation algorithm flowchart.

also imposes the validity ranges for distances and angles to be used in the validation procedure. Parsing of data is performed by calling the following function:

```
int parse_data()
```

### First validation

The first validation procedure aims to find  $fk$  consecutive consistent values, where  $fk$  is a tunable coefficient, checking consistency of both distances and angles. If it succeeds, the algorithm proceeds to the next validation phase; otherwise, if a non consistent

values is found before collecting  $fk$  consecutive consistent values, the procedure restarts. Consistency of the values is checked by using the validity ranges defined in the parsing function:

```
if current_value  $\in$  (last_value  $\mp$  validity_range)
then current_value is valid
```

Angles values are considered in modulus, since there are points in which they can change from  $-90$  to  $+90$ . Once  $fk$  consecutive consistent values are found, and the algorithm can move to the next phase, the last arrived values are used as sample values for the next validation procedure. To execute the first validation algorithm we have to call the following function:

```
int first_validation()
```

### Step validation

The step validation procedure compares each new arriving distance measure with the sample value:

```
if current_value  $\in$  (sample_value  $\mp$  validity_range)
then current_value is valid
```

If the measure is consistent, then the distance and the angle values can be used to compute the set-point, and so they are marked as refer values for the generating set-point algorithm. If a non consistent measure is found, the values are discarded, the validity ranges are enlarged, and the check is repeated by using the next arriving measure. After that  $sk$  non valid measures are found, the first validation procedure must be repeated. Also  $sk$  is a tunable coefficient. The step validation algorithm function can be called with the following string of code:

```
int step_validation()
```

## 2.2 Flux Line search technique

The first algorithm we are going to present is based on the fact that the ARTVA transmitter behave like a magnetic dipole. The main idea is to exploit this characteristic to align the drone to a flux line, and make the vehicle follow it until it reaches the beacon transmitter. Practically speaking, at each new ARTVA data received, we want the drone to compensate its yaw inclination with respect to the line tangent to the flux ellipse, and to move along that direction, as it is shown in Figure 2.3. The output of the algorithm will be a velocity set-point (and also a yaw correction).

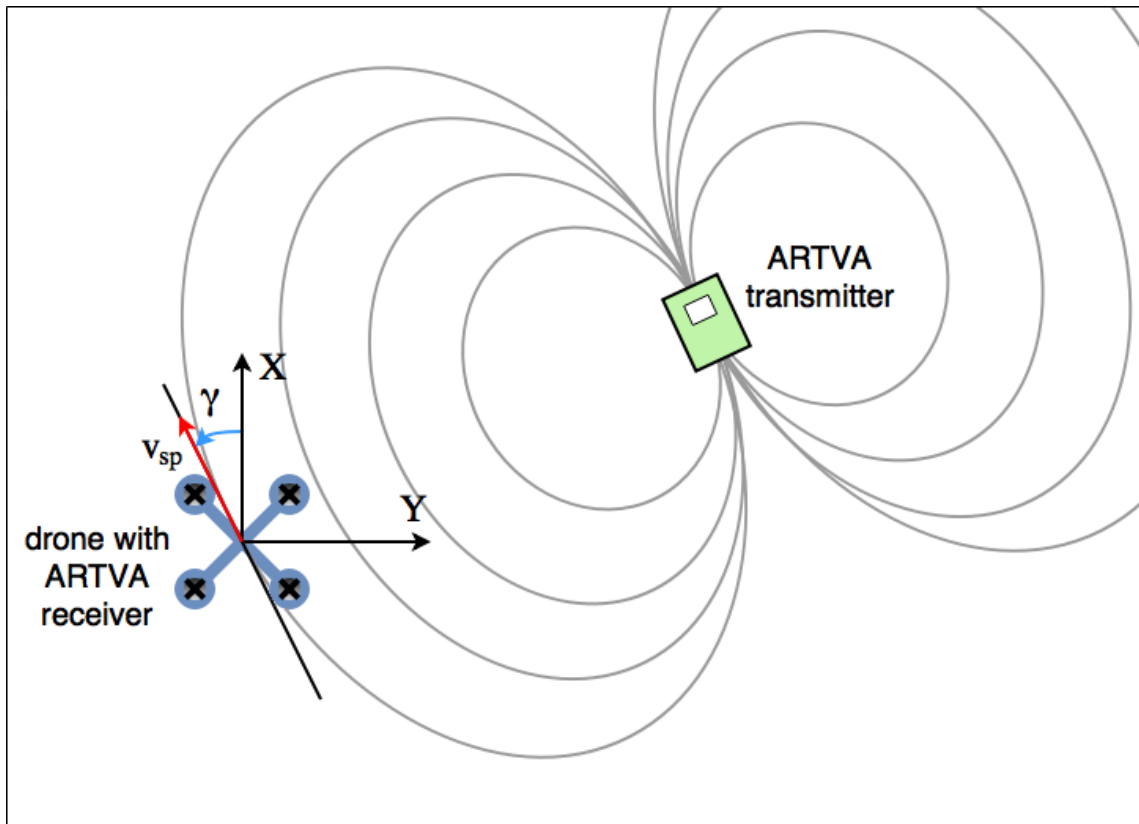


**Figure 2.3.** Flux Line search technique operation: the red arrow represents the velocity set-point, the light blue arrows represents the yaw correction.

### 2.2.1 Mathematical description

The drone is guided toward the victim by means of the following reference velocity[4]:

$$v^*(\tau) = v_\delta(k) \frac{v_{max} K d(k)}{\sqrt{1 + K^2 d^2}} \quad (2.1)$$

valid  $\forall \tau \in [k, k + \Delta T]$ , where

$$v_\delta = \begin{bmatrix} \cos \delta(k) \\ \sin \delta(k) \\ 0 \end{bmatrix}$$

Moreover,  $K$  is a tunable coefficient, while  $v_{max}$  represents the drone's maximum speed in the horizontal plane. The yaw reference, designed to make the  $X$ -axis of the drone's reference frame aligned with the direction of  $v^*(\tau)$ , is computed by means of the following law:

$$\psi^*(\tau) = \psi(k) + \delta(k) \quad (2.2)$$

valid  $\forall \tau \in [k, k + \Delta T]$

### Stability analysis

For the purpose of analysing the stability of the search based on flux lines, we can represent the transmitter's nominal magnetic field as follows:

$$H = \frac{1}{4\pi r^5} Am \quad (2.3)$$

where

$$A = \begin{bmatrix} 2x^2 - y^2 - z^2 & 3xy & 3xz \\ 3xy & 2y^2 - x^2 - z^2 & 3yz \\ 3xz & 3yz & 2z^2 - x^2 - y^2 \end{bmatrix}$$

and  $r^2 = x^2 + y^2 + z^2$  is the actual Cartesian distance from the transmitter to the receiver, and  $m = [m_x \ m_y \ m_z]^T$  represents the transmitter magnetic moment, in the inertial reference frame. Furthermore, to reduce the calculus complexity, we can centre, without loss of generality, the inertial frame  $\mathcal{F}_i$  on the transmitter, which is generically oriented on the inertial  $x_i$ - $z_i$  plane. Given  $H_{x_i y_i} = [H_{x_i} \ H_{y_i}]^T$ , projection of  $H$  on the inertial  $x_i$ - $z_i$  plane, the following analysis is conducted by imposing the  $X$ -axis of the drone's reference frame aligned with the  $H_{x_i y_i}$  vector, the  $Z$ -axis of the drone's reference

frame parallel to the inertial  $z_i$ -axis, and the  $Y$ -axis of the drone's reference frame aligned consequently. Finally, the centre  $O$  of the drone's reference frame is placed on the inertial  $x_i$ - $y_i$  plane at the coordinates identified by means of the couple  $(x, y)$ . Given the time instant  $k$ , it is possible to introduce a polar coordinate change:

$$\begin{bmatrix} x(k) \\ y(k) \end{bmatrix} = \begin{bmatrix} \rho(k) \cos \theta(k) \\ \rho(k) \sin \theta(k) \end{bmatrix} \quad (2.4)$$

Then, the vector  $H_{x_i y_i}$  can be described in terms of its parallel and perpendicular components with respect to the radius  $\rho(k)$ :

$$\begin{bmatrix} H_{\parallel} \\ H_{\perp} \end{bmatrix} = \begin{bmatrix} \cos \theta(k) & \sin \theta(k) \\ -\sin \theta(k) & \cos \theta(k) \end{bmatrix} \begin{bmatrix} H_{x_i} \\ H_{y_i} \end{bmatrix} \quad (2.5)$$

Assuming that the inertial drone's reference velocity  $v_i^*(k)$  is taken along the direction of the vector  $H_{x_i y_i}$  with modulus  $\|v^*(k)\| > 0$ , we have that:

$$\begin{bmatrix} v_{i_x}^*(k) \\ v_{i_y}^*(k) \end{bmatrix} = \frac{\|v^*(k)\|}{\|H_{x_i y_i}\|} \begin{bmatrix} H_{x_i} \\ H_{y_i} \end{bmatrix} \quad (2.6)$$

which can also be expressed in terms of parallel and perpendicular components with respect to the radius  $\rho(k)$ :

$$\begin{bmatrix} v_{i_{\parallel}}^*(k) \\ v_{i_{\perp}}^*(k) \end{bmatrix} = \frac{\|v^*(k)\|}{\|H_{x_i y_i}\|} \begin{bmatrix} H_{\parallel} \\ H_{\perp} \end{bmatrix} \quad (2.7)$$

The angle  $\theta(k)$  can be changed if and only if the perpendicular component of the velocity is different from zero.

$$\rho \dot{\theta}(k) = v_{i_{\perp}}^*(k) = \frac{\|v^*(k)\|}{\|H_{x_i y_i}\|} m_x \rho^2(k) \cdot \sin \theta(k) \quad (2.8)$$

**Proposition 1** For any initial condition  $(\rho(0), \theta(0))$  with  $\rho(0) > 0$  and  $\theta(0) \neq 0$ , the



tracking of the references (2.1) and (2.2) guarantees that

$$\lim_{k \rightarrow \infty} \theta(k) = \pi$$

**Proposition 2** For any initial condition  $(\rho(0), \theta(0))$  with  $\rho(0) > 0$  and  $\frac{\pi}{2} < \theta(0) < \frac{3\pi}{2}$ , the tracking of the references (2.1) and (2.2) guarantees that

$$\lim_{k \rightarrow \infty} \rho(k) = 0$$

**Remark** The composition of Proposition 1 and Proposition 2 says that if the search starts with initial conditions given by  $\rho > 0$  and  $\theta \in (\frac{-\pi}{2}, \frac{\pi}{2})$ , the radius increases until the angle  $\theta$  does not reach the compact domain  $[\frac{\pi}{2}, \frac{3\pi}{2}]$ . This problem is solved with the direction inversion procedure later described.

### 2.2.2 Implementation

The Flux Line set-point generation algorithm follows the steps below:

**Direction check** Once every  $ck$  data received, where  $ck$  is a tunable coefficient, stores a distance value. Each time new data pass the validation algorithm, compares the distance value of the new data with the last stored one. If the new value is greater than the stored one, changes sign to the formula that computes the set-point. Moreover, only for the current iteration, instead of computing a new velocity set-point, the algorithm will publish the last computed set-point changed in sign. In this way the drone will come back to the previous position before the algorithm starts computing new set-point values in the opposite direction.

**Yaw correction** Computes the yaw correction to be applied to the drone if the angle values received from ARTVA is greater than a certain threshold:

if  $angle\_value > threshold$  then apply the yaw correction

The yaw correction is saturated to a maximum value in such a way to be applied

gradually each time a new set-point is given to the controller:

if  $angle\_value \leq yaw\_correction\_max$  then  $yaw\_correction = angle\_value$   
 else  $yaw\_correction = yaw\_correction\_max$

In this way, we avoid to have non-consistent consecutive ARTVA measures, which will create difficulties in the data validation phase.

**Velocity set-point computation** Uses the current distance value to compute the velocity set-point, so that the closer the drone is to the beacon transmitter, the lower is the imposed velocity. Also the generated velocity is saturated to a maximum value:

if  $distance\_value \leq velocity\_max$  then  $velocity\_set\_point = distance\_value$   
 else  $velocity\_set\_point = velocity\_max$

In order to be passed to the controller, the velocity set-point value, which is intended in the direction tangent to the flux ellipse, must be decomposed along the  $X$  and  $Y$  directions of the drone body frame:

$$\begin{aligned} v_{spx} &= sign \cdot v_{sat} \cdot \cos(\delta) \\ v_{spy} &= sign \cdot v_{sat} \cdot \sin(\delta) \end{aligned} \tag{2.9}$$

where  $\delta$ , which is the angle value received from ARTVA, is equal to zero if the yaw angle has been completely compensated.

**Reference system transformation** Transforms the reference system from the one in agreement with the body to the inertial one:

$$\begin{aligned} v_{spX} &= v_{spx} \cdot \cos(\gamma) + v_{spy} \cdot \sin(\gamma) \\ v_{spY} &= -v_{spx} \cdot \sin(\gamma) + v_{spy} \cdot \cos(\gamma) \end{aligned} \tag{2.10}$$

where  $\gamma$  is the residual value of the yaw angle of the drone after the correction.

Finally, the algorithm publishes the two values of the velocity set-point and the value of yaw correction to a topic from which the controller can read them.

## 2.3 Extremum Seeking search technique

The next presented algorithm is based on the Extremum Seeking Control, a control technique which aim to select the set-point to keep the output at the extremum value (maximum or minimum). In our case, we want to use this kind of control to search for the minimum value of the distance from the beacon transmitter.

### 2.3.1 SISO scheme and linear analysis

#### Extremum Seeking for a static map

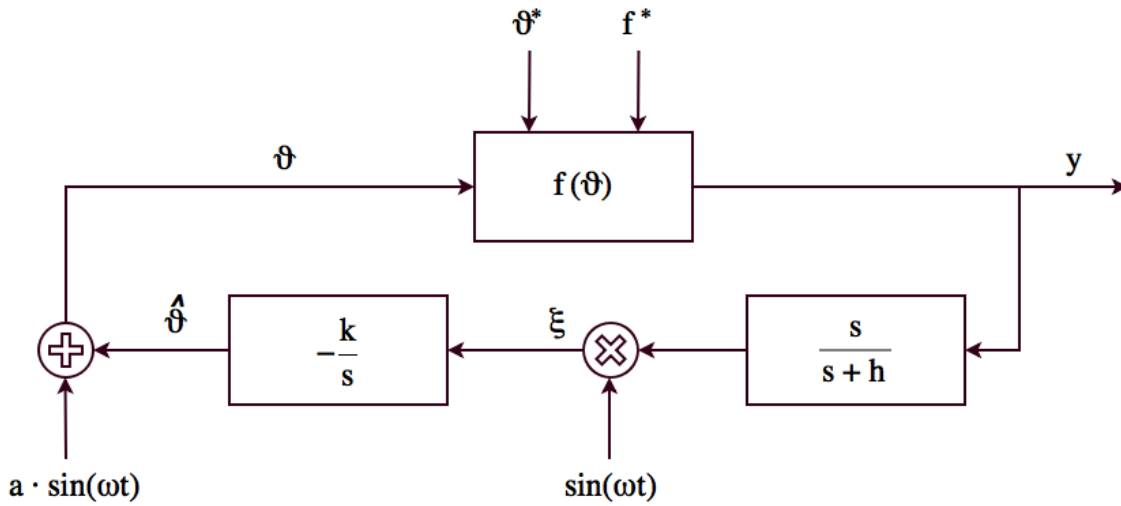


**Figure 2.4.** Extremum Seeking Control scheme for a static map.

Considering the Extremum Seeking scheme for a static map[5], represented in Figure 2.4, we have that:

$$f(\vartheta) = f^* + \frac{f''}{2}(\vartheta - \vartheta^*)^2 \quad (2.11)$$

where  $f'' > 0$ . If  $f'' < 0$ , replace  $k$  ( $k > 0$ ) with  $-k$ , so to obtain  $f'' > 0$ . The purpose is to make  $\vartheta - \vartheta^*$  as small as possible, so that the output  $y = f(\vartheta)$  is driven to its minimum. The perturbation signal  $a \cdot \sin(\omega t)$  helps to get a measure of gradient information of  $f(\vartheta)$ . Defining the following quantities:

- $\vartheta^*$ : optimal input (unknown);
- $\hat{\vartheta}$ : estimation of the optimal input;

- $\tilde{\vartheta} = \vartheta^* - \hat{\vartheta}$ : estimation error;

We can write:

$$\vartheta^* - \hat{\vartheta} = a \cdot \sin(\omega t) - \tilde{\vartheta} \quad (2.12)$$

From (2.11) and (2.12) we obtain:

$$\begin{aligned} y &= f^* + \frac{f''}{2}(a \cdot \sin(\omega t) - \tilde{\vartheta})^2 \\ &= f^* + \frac{f''}{2}a^2 \cdot \sin^2(\omega t) + \frac{f''}{2}\tilde{\vartheta}^2 - f''\tilde{\vartheta}a \cdot \sin(\omega t) \\ &= f^* + \frac{f''}{4}a^2 + \frac{f''}{4}a^2 \cdot \cos(2\omega t) + \frac{f''}{2}\tilde{\vartheta}^2 - f''\tilde{\vartheta}a \cdot \sin(\omega t) \end{aligned} \quad (2.13)$$

The high-pass filter  $\frac{s}{s+h}$  serves to remove  $f^*$

$$y_f = \frac{s}{s+h}y \approx \frac{f''}{4}a^2 \cdot \cos(2\omega t) + \frac{f''}{2}\tilde{\vartheta}^2 - f''\tilde{\vartheta}a \cdot \sin(\omega t) \quad (2.14)$$

Then the signal is demodulated by  $\sin(\omega t)$

$$\xi = \frac{f''}{4}a^2 \cdot \cos(2\omega t) \sin(\omega t) + \frac{f''}{2}\tilde{\vartheta}^2 \cdot \sin(\omega t) - f''\tilde{\vartheta}a \cdot \sin^2(\omega t) \quad (2.15)$$

From (2.15), applying some trigonometric formulas, we can find:

$$\xi = -\frac{f''}{2}\tilde{\vartheta}a + \frac{f''}{2}\tilde{\vartheta}a \cdot \cos(2\omega t) + \frac{f''}{8}a^2(\sin(\omega t) - \sin(3\omega t)) + \frac{f''}{2}\tilde{\vartheta}^2 \cdot \sin(\omega t) \quad (2.16)$$

Since  $\vartheta^*$  is constant,  $\dot{\tilde{\vartheta}} = -\dot{\hat{\vartheta}}$ . So, we get:

$$\tilde{\vartheta} \approx \frac{k}{s} \left[ -\frac{f''}{2}\tilde{\vartheta}a + \frac{f''}{2}\tilde{\vartheta} \cdot \cos(2\omega t) + \frac{f''}{8}a^2(\sin(\omega t) - \sin(3\omega t)) + \frac{f''}{2}\tilde{\vartheta}^2 \cdot \sin(\omega t) \right] \quad (2.17)$$

Neglecting the last term of (2.17), since it is quadratic in  $\tilde{\vartheta}$ , we obtain:

$$\tilde{\vartheta} \approx \frac{k}{s} \left[ -\frac{f''}{2}\tilde{\vartheta}a + \frac{f''}{2}\tilde{\vartheta} \cdot \cos(2\omega t) + \frac{f''}{8}a^2(\sin(\omega t) - \sin(3\omega t)) \right] \quad (2.18)$$

Since the last two terms of (2.18) are high frequency signals, an integretor will nearly cancels them. We can neglect them obtaining so:

$$\tilde{\vartheta} \approx \frac{k}{s} \left[ -\frac{f''}{2}\tilde{\vartheta} \right] \Rightarrow \dot{\tilde{\vartheta}} = -k\frac{f''}{2}\tilde{\vartheta} \quad (2.19)$$

Since  $kf'' > 0$ , the system is stable and  $\tilde{\vartheta}$  goes to zero.

**Remark** These approximations works only when  $\omega$  is large (in a qualitative sense)

relative to  $k$ ,  $a$ ,  $h$ , and  $f''$ ,

**Theorem (Extremum Seeking)** For the presented system, the output error  $y - f^*$  achieves local exponential convergence to an  $O(a^2 + \frac{1}{\omega^2})$  neighbourhood of the origin, provided the perturbation frequency  $\omega$  is sufficiently large, and  $\frac{1}{(1+L(s))}$  is asymptotically stable, where  $L(s) = \frac{ka f''}{2s}$ .

### Single parameter Extremum Seeking for plants with dynamics

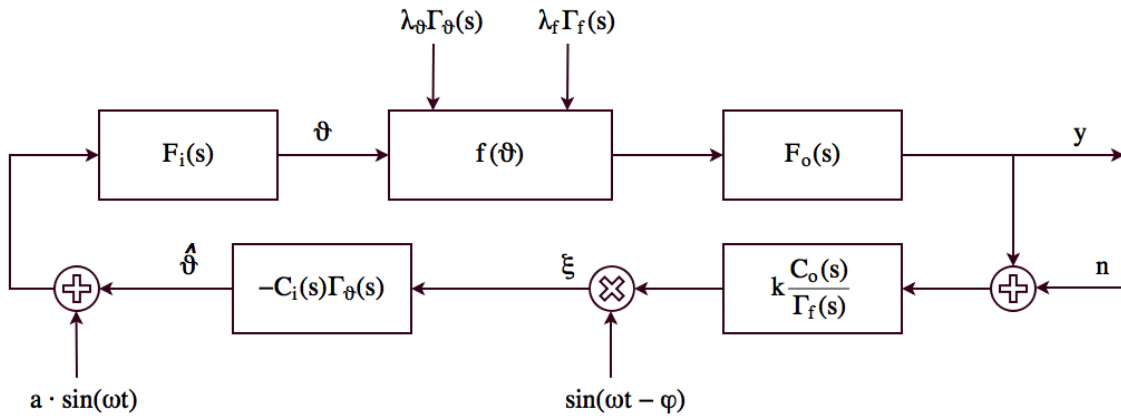


**Figure 2.5.** Single parameter Extremum Seeking Control scheme for plants with dynamics.

The scheme in Figure 2.5 shows a non-linear plant with linear dynamics along with the Extremum Seeking loop. We have that:

$$f(\vartheta) = f^*(t) + \frac{f''}{2}(\vartheta - \vartheta^*(t))^2 \quad (2.20)$$

where  $f'' > 0$ , constant and unknown. The purpose is to make  $\vartheta - \vartheta^*$  as small as possible, so that the output  $F_o(s)[f(\vartheta)]$  is driven to its extremum  $F_o(s)[f^*(\vartheta)]$ . The optimal input and output,  $\vartheta^*$  and  $f^*$ , may be time-varying and their Laplace transforms are expressed as follows:

$$\begin{aligned} \mathcal{L}\{\vartheta^*(t)\} &= \lambda_\vartheta \Gamma_\vartheta(s) \\ \mathcal{L}\{f^*(t)\} &= \lambda_f \Gamma_f(s) \end{aligned} \quad (2.21)$$

If  $\vartheta^*$  and  $f^*$  are constants, from (2.21) we can find:

$$\begin{aligned}\mathcal{L}\{\vartheta^*(t)\} &= \frac{\lambda_\vartheta}{s} \\ \mathcal{L}\{f^*(t)\} &= \frac{\lambda_f}{s}\end{aligned}\tag{2.22}$$

While  $\lambda_\vartheta$  and  $\lambda_f$  are unknown, the Laplace transform of  $\vartheta^*$  and  $f^*$  is known, and is included in the washout filter:

$$\frac{C_o(s)}{\Gamma_f(s)} = \frac{s}{s+h}\tag{2.23}$$

and in the estimation algorithm:

$$C_i(s)\Gamma_\vartheta(s) = \frac{1}{s}\tag{2.24}$$

The inclusion of  $\Gamma_\vartheta(s)$  and  $\Gamma_f(s)$  in the respective blocks in the feedback branch follows the internal model principle. When applied, in a very generalized manner, to the Extremum Seeking problem, it allows us to track time-varying maxima or minima.

The compensators  $C_i(s)$  and  $C_o(s)$  are crucial design tools for satisfying stability conditions and achieving desired convergence rates.

## 2.3.2 Non-local stability of non-linear case

### Introduction

Considering the following non-linear system[6]:

$$\begin{aligned}\dot{x} &= f(x, u) \\ y &= h(x)\end{aligned}\tag{2.25}$$

and suppose that exist a unique  $x^*$  such that  $y^* = h(x^*)$  is the extremum of the map  $h(\cdot)$ . Assume, due to uncertainty, that neither  $x^*$  nor  $h(\cdot)$  are precisely known. The objective is to force the solution of the closed-loop system to eventually converge to  $x^*$  and to do so without any precise knowledge about  $x^*$  or  $h(\cdot)$ .

The purpose is to show that, under appropriate conditions, the Extremum Seeking controller achieves semi-global practical stability of the closed-loop system. In other words, given an arbitrarily large set of initial conditions  $B_\Delta$  and an arbitrarily small neighbourhoods  $B_\nu$  of the state  $x^*$  where the output achieves its extremum  $y^* = h(x^*)$ , it is

possible to adjust the controller parameters so that all solutions starting from the set  $B_\Delta$  eventually converge to  $B_v$ .

### Preliminaries

Given the following system:

$$\dot{x} = f(t, x, \epsilon) \quad (2.26)$$

with  $x \in \mathbb{R}^n$ ,  $t \in \mathbb{R} > 0$ ,  $\epsilon \in \mathbb{R}^l > 0$ , the stability of (2.26) can depend in an intricate way on the parameters vector  $\epsilon$ .

**Definition (Semi-Global Practical Asymptotic Stability)** System (2.26) is said to be semi-global practical asymptotically (SPA) stable, uniformly in  $(\epsilon_1, \epsilon_2, \dots, \epsilon_j)$ ,  $j \in \{1, 2, \dots, l\}$ , if there exists  $\beta \in \mathcal{KL}$  such that the following holds: for each pair of strictly positive real numbers  $(\Delta, v)$ , there exist real numbers  $\epsilon_k^* = \epsilon_k^*(\Delta, v) > 0$ ,  $k = 1, 2, \dots, j$ , and for each fixed  $\epsilon_k \in (0, \epsilon_k^*)$ ,  $k = 1, 2, \dots, j$ , there exist  $\epsilon_i = \epsilon_i(\epsilon_1, \epsilon_2, \dots, \epsilon_{i-1}, \Delta, v)$ , with  $i = j + 1, j + 2, \dots, l$ , such that the solutions of the system with the so constructed parameters  $\epsilon = (\epsilon_1, \epsilon_2, \dots, \epsilon_l)$  satisfy:

$$|x(t)| \leq \beta(|x_0|, (\epsilon_1 \cdot \epsilon_2 \cdot \dots \cdot \epsilon_l)(t - t_0)) + v \quad (2.27)$$

for all  $t \geq t_0 \geq 0$ ,  $x(t_0) = x_0$ , with  $|x_0| \leq \Delta$ . If we have that  $j = l$ , then we can say that the system is SPA stable, uniformly in  $\epsilon$ .

### Problem formulation

Considering the following single-input single-output (SISO) non-linear model:

$$\begin{aligned} \dot{x} &= f(x, u) \\ y &= h(x) \end{aligned} \quad (2.28)$$

with  $f : \mathbb{R}^n \times \mathbb{R} \rightarrow \mathbb{R}^n$ ,  $f \in C$ , and  $h : \mathbb{R}^n \rightarrow \mathbb{R}$ ,  $h \in C$ . Considering a family of control laws of the following form:

$$u = \alpha(x, \vartheta) \quad (2.29)$$

with  $\vartheta \in \mathbb{R}$ , scalar parameter. The closed loop system is then:

$$\dot{x} = f(x, \alpha(x, \vartheta)) \quad (2.30)$$

The requirement that  $\vartheta$  is scalar and that the system is SISO is to simplify the presentation.

**Assumption 1** There exists a function  $I : \mathbb{R} \rightarrow \mathbb{R}^n$  such that

$$f(x, \alpha(x, \vartheta)) = 0 \quad (2.31)$$

if and only if  $x = I(\vartheta)$ .

**Assumption 2** For each  $\vartheta \in \mathbb{R}$ , the equilibrium  $x = I(\vartheta)$  of the closed-loop system is globally asymptotically stable, uniformly in  $\vartheta$ .

**Assumption 3** Denoting  $Q(\cdot) = h \circ I$ , there exists a unique  $\vartheta^*$  maximizing  $Q(\cdot)$ , and the following holds:

$$Q'(\vartheta^*) = 0, \quad Q''(\vartheta^*) < 0 \quad (2.32)$$

### Main results

Considering the first order Extremum Seeking control scheme shown in Figure 2.6:

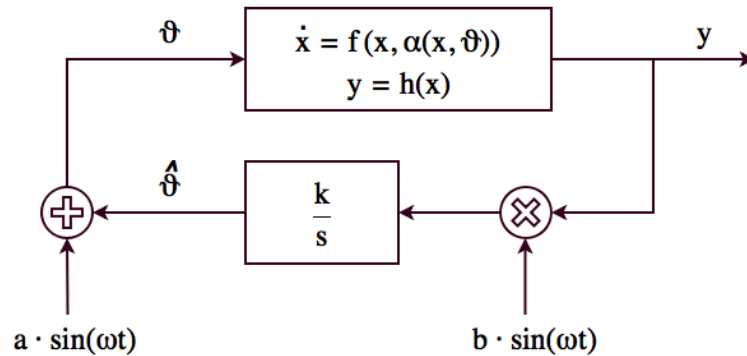


**Figure 2.6.** First order Extremum Seeking control scheme.

The dynamics of the system are the following:

$$\begin{aligned} \dot{x} &= f(x, \alpha(x, \hat{\vartheta} + a \cdot \sin(\omega t))) \\ \dot{\hat{\vartheta}} &= kh(x)b \cdot \sin(\omega t) \end{aligned} \quad (2.33)$$



Introducing a change of coordinates:

$$\begin{aligned}\tilde{x} &= x - x^* \\ \tilde{\vartheta} &= \vartheta - \vartheta^*\end{aligned}\tag{2.34}$$

we note that the point  $(x^*, \vartheta^*)$  is in general not an equilibrium point of the system. However, our purpose is to show that the system in new coordinate is SPA stable, which ensure Extremum Seeking. The system (2.33) with the new coordinates (2.34) takes the following form:

$$\begin{aligned}\dot{\tilde{x}} &= f(\tilde{x} + x^*, \alpha(\tilde{x} + x^*, \tilde{\vartheta} + \vartheta^* + a \cdot \sin(\omega t))) \\ \dot{\tilde{\vartheta}} &= kh(\tilde{x} + x^*)b \cdot \sin(\omega t)\end{aligned}\tag{2.35}$$

Defining now:

$$\begin{aligned}k &= \omega \delta K \\ \sigma &= \omega t\end{aligned}\tag{2.36}$$

where  $\omega$  and  $\sigma$  are small parameters,  $K > 0$  is fixed, and replacing (2.36) in (2.35), we obtain the system equations expanded in time  $\sigma$ :

$$\begin{aligned}\omega \frac{d\tilde{x}}{d\sigma} &= f(\tilde{x} + x^*, \alpha(\tilde{x} + x^*, \tilde{\vartheta} + \vartheta^* + a \cdot \sin(\sigma))) \\ \frac{d\tilde{\vartheta}}{d\sigma} &= \delta K h(\tilde{x} + x^*)b \cdot \sin(\sigma)\end{aligned}\tag{2.37}$$

For simplicity of representation, we let  $b = a$ , so that the vector of parameters is the following:

$$\epsilon = [a^2 \ \delta \ \omega]^T\tag{2.38}$$

System (2.37) has a two-time-scale structure and the first main result is proved by applying the singular perturbations and averaging methods.

**Theorem** Suppose that assumptions 1-3 hold. Then, the closed-loop system (2.37), when  $b = a$  and with parameter vector (2.38), is SPA stable, uniformly in  $(a^2, \delta)$ .

Considering now the higher order Extremum Seeking control scheme represented in Figure 2.7, supposing  $W_L(s) = (\frac{\omega_l}{s} + \omega_l)$  and  $W_H(s) = 1$ . The Extremum Seeking controller contains an integrator and a low-pass filter. The low-pass filter is useful when we need

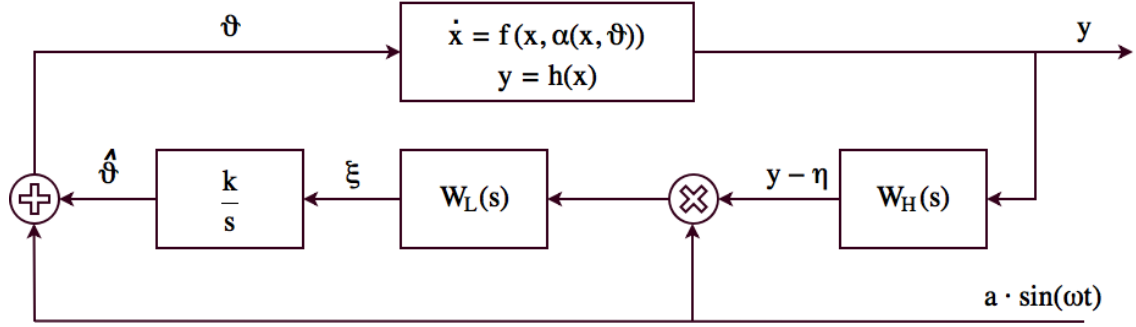


**Figure 2.7.** Higher order Extremum Seeking control scheme.

to filter out high frequency measurement noise in the system. Moreover, tuning the filter parameter  $\omega_l$  may lead to a possible improvement in the transient response.

The following equations describe the closed-loop system under the above conditions:

$$\begin{aligned}
 \dot{x} &= f(x, \alpha(x, \hat{\vartheta} + a \cdot \sin(\omega t))) \\
 \dot{\hat{\vartheta}} &= k\xi \\
 \dot{\xi} &= -\omega_l \xi + \omega_l h(x) a \cdot \sin(\omega t)
 \end{aligned} \tag{2.39}$$

Introducing a change of coordinates:

$$\begin{aligned}
 \tilde{x} &= x - x^* \\
 \tilde{\vartheta} &= \vartheta - \vartheta^* \\
 \tilde{\xi} &= \xi
 \end{aligned} \tag{2.40}$$

system (2.39) with the new coordinates (2.40) takes the following form:

$$\begin{aligned}
 \dot{\tilde{x}} &= f(\tilde{x} + x^*, \alpha(\tilde{x} + x^*, \tilde{\vartheta} + \vartheta^* + a \cdot \sin(\omega t))) \\
 \dot{\tilde{\vartheta}} &= k\tilde{\xi} \\
 \dot{\tilde{\xi}} &= -\omega_l [\tilde{\xi} - h(\tilde{x} + x^*) a \cdot \sin(\omega t)]
 \end{aligned} \tag{2.41}$$

Defining now:

$$\begin{aligned}
 \omega_l &= \omega \delta \omega_L \\
 k &= \omega \delta K \\
 \sigma &= \omega t
 \end{aligned} \tag{2.42}$$

where  $\omega$  and  $\sigma$  are small parameters,  $\omega_L$  and  $K > 0$  are fixed, and replacing (2.42) in (2.41), we obtain the system equations expanded in time  $\sigma$ :

$$\begin{aligned}\omega \frac{d\tilde{x}}{d\sigma} &= f(\tilde{x} + x^*, \alpha(\tilde{x} + x^*, \tilde{\vartheta} + \vartheta^* + a \cdot \sin(\sigma))) \\ \frac{d\tilde{\vartheta}}{d\sigma} &= \delta K \tilde{\xi} \\ \frac{d\tilde{\xi}}{d\sigma} &= -\delta \omega_L [\tilde{\xi} - h(\tilde{x} + x^*) a \cdot \sin(\sigma)]\end{aligned}\tag{2.43}$$

With the same parameter vector  $\epsilon$  defined in (2.38)

**Theorem** Suppose that assumptions 1-3 hold. Then, the closed-loop system (2.43), with parameter vector (2.38), is SPA stable, uniformly in  $a^2$ .

### 2.3.3 Hybrid Extremum Seeking Control

The next presented algorithm is based on an Hybrid Extremum Seeking Control (HESC). An hybrid dynamical system[7] is modelled as follows:

$$\begin{aligned}x \in C \quad \dot{x} &= f(x) \\ x \in D \quad x^+ &= g(x)\end{aligned}\tag{2.44}$$

The state  $x$  of the hybrid system can change according to a differential equation  $\dot{x} = f(x)$  and according to a difference equation  $x^+ = g(x)$ . The behaviour of a dynamical system which can be described by a differential equation is referred to as flow, while the behaviour of a dynamical system which can be described by a difference equation is referred to as jump. The objects involved in model (2.44) are:

- the flow set  $C$ ,
- the flow map  $f$ ,
- the jump set  $D$ ,
- the jump map  $g$ .

Considering now the model of the HESC[8], and assuming that the time domain is described by continuous-time interval parametrized by  $\tau \in [0, T)$ , with  $T > 0$ , and

discrete-time instants  $j \in \mathbb{N}$ , the flow map is described by the following equations:

$$\begin{aligned}
\dot{p}_x &= \bar{v}_x \\
\dot{v}_x &= -k_{1x}\bar{v}_x - k_{2x}\bar{w}_x \\
\dot{w}_x &= 0 \\
\dot{p}_y &= \bar{v}_y \\
\dot{v}_y &= -k_{1y}\bar{v}_y - k_{2y}\bar{w}_y \\
\dot{w}_y &= 0 \\
\dot{h}^* &= 0 \\
\dot{\psi}^* &= 0 \\
\dot{\tau} &= 1
\end{aligned} \tag{2.45}$$

where  $k_{1x}$ ,  $k_{2x}$ ,  $k_{1y}$  and  $k_{2y}$  are positive constants to be defined. The flow set is defined as:

$$(\dot{p}_x, \dot{v}_x, \dot{w}_x, \dot{p}_y, \dot{v}_y, \dot{w}_y, \dot{h}^*, \dot{\psi}^*), \dot{\tau} \in \mathbb{R}^8 \times [0, T] \tag{2.46}$$

Indicating with  $d$  the distance values and with  $\delta$  the angle values obtained from ARTVA, the jump map is described as follows:

$$\begin{aligned}
\bar{p}_x^+ &= \bar{p}_x \\
\bar{v}_x^+ &= \bar{v}_x \\
\bar{w}_x^+ &= \frac{1}{n} \sum_{i=j+1-n}^j d(i) \sin(i\omega_x T) \\
\bar{p}_y^+ &= \bar{p}_y \\
\bar{v}_y^+ &= \bar{v}_y \\
\bar{w}_y^+ &= \frac{1}{n} \sum_{i=j+1-n}^j d(i) \sin(i\omega_y T) \\
h^{*+} &= h^* \\
\psi^{*+} &= \psi + \delta \\
\tau^+ &= 0
\end{aligned} \tag{2.47}$$

where  $j \in \mathbb{N}$  indicates the current jump, and also the instant when a new ARTVA data is received,  $\omega_x$  and  $\omega_y \in \mathbb{R}_{>0}$ ,  $n \in \mathbb{N}$ . The jump set is defined as:

$$(\dot{\bar{p}}_x, \dot{v}_x, \dot{w}_x, \dot{\bar{p}}_y, \dot{v}_y, \dot{w}_y, \dot{h}^*, \dot{\psi}^*), \dot{\tau} \in \mathbb{R}^8 \times T \quad (2.48)$$

Finally, given the composite time  $t = \tau + jT$ , the output of the controller are the following reference positions:

$$\begin{aligned} p_x^*(t) &= \bar{p}_x(t) + \rho_x \cos(\omega_x t) \\ p_y^*(t) &= \bar{p}_y(t) + \rho_y \sin(\omega_y t) \end{aligned} \quad (2.49)$$

where  $\rho_x$  and  $\rho_y$  are positive real constants to be defined. By choosing  $\rho_x = \rho_y$  and  $\omega_x = \omega_y$ , we can drive the drone to describe a series of circles, with radius  $\rho_x = \rho_y$ , during its trajectory; alternatively by imposing  $\omega_y = 2\omega_x$  and  $\rho_x = 2\rho_y$ , we can drive the drone to describe a series of eight-shaped paths in its trajectory. This approach could be useful to detect the exact position of the buried victim when the distance values received from ARTVA are small.

### Stability analysis

We have to introduce some definitions in order to analyse the stability of the controller.

**Definition (Terrain)** The avalanche terrain is described by the piece-wise continuous map

$$z = h_a(x, y) \quad (2.50)$$

where  $h_a(0, 0) > 0$  and  $x$ ,  $y$  and  $z$  are the coordinates of the inertial reference frame  $\mathcal{F}_i(O_i, x_i, y_i, z_i)$ .

**Definition (Minima Set)** Given the attitude of the transmitter and the receiver, defined with  $\mathcal{R}_t$  and  $\mathcal{R}$  respectively, given the avalanche terrain defined by (2.50), then, for any positive constant  $\bar{d}$ , the minima set  $\Omega$  is defined as:

$$\Omega := \{(x, y) \in \mathbb{R}^2 : \nabla d(x, y, d + h_a(x, y)) = 0, \mathcal{H}(x, y, d + h_a(x, y)) > 0\} \quad (2.51)$$

where  $\mathcal{H}(x, y, d + h_a(x, y))$  represents the Hessian matrix of  $d$  valued at  $(x, y, d +$

$h_a(x, y)$ .

**Definition (Minima Domain)** For each element  $(\bar{x}, \bar{y}) \in \Omega$ , the minima domain  $\mathcal{D}_{(\bar{x}, \bar{y})}$  is defined as the compact set

$$\mathcal{D}_{(\bar{x}, \bar{y})} := \left\{ (x, y) \in \mathbb{R}^2 : \nabla d(x - \bar{x}, y - \bar{y}, d + h_a(x - \bar{x}, y - \bar{y})) \times \begin{bmatrix} x - \bar{x} \\ y - \bar{y} \end{bmatrix} > 0 \right\} \quad (2.52)$$

where  $(\bar{x}, \bar{y}) \in \mathcal{D}_{(\bar{x}, \bar{y})}$ .

The validity of the HESC is based on the following assumptions:

**Assuption (Periodicity)** The pulsations  $\omega_x$  and  $\omega_y$  and the number of samples  $n$  are such that

$$\begin{aligned} \frac{1}{n} \sum_{i=j+1-n}^j \sin(i\omega_x T) &= 0 \\ \frac{1}{n} \sum_{i=j+1-n}^j \sin(i\omega_y T) &= 0 \end{aligned} \quad (2.53)$$

**Assuption (Persistent Excitation)** The pulsations  $\omega_x$  and  $\omega_y$  are such that there exist two positive constants  $\alpha_x$  and  $\alpha_y$  such that

$$\begin{aligned} \frac{1}{n} \sum_{i=j+1-n}^j \sin^2(i\omega_x T) &> \alpha_x \\ \frac{1}{n} \sum_{i=j+1-n}^j \sin^2(i\omega_y T) &> \alpha_y \end{aligned} \quad (2.54)$$

and furthermore

$$\frac{1}{n} \sum_{i=j+1-n}^j \sin(i\omega_x T) \sin(i\omega_y T) = 0 \quad (2.55)$$

Now we can conclude that:

**Theorem** Given the HESC controller (2.45)-(2.47) and the position of the drone defined by  $p = [p_x^*, p_y^*, \bar{d} + h_a(x, y)]$ , and assuming  $\|w\| = 0$ , then, for any  $\rho > 0$  such that  $\mathcal{B}_\rho(\bar{x}, \bar{y}) \subset \mathcal{D}_{(\bar{x}, \bar{y})}$ , there exist two positive constants  $\bar{\rho}_x$  and  $\bar{\rho}_y$  such that, for any  $(\rho_x^*(0), \rho_y^*(0)) \in \mathcal{B}_\rho(\bar{x}, \bar{y})$  and for all  $0 < \rho_x < \bar{\rho}_x$  and  $0 < \rho_y < \bar{\rho}_y$ , the point  $(\bar{x}, \bar{y})$  is locally asymptotically stable.

The term  $\mathcal{B}_\rho(\bar{x}, \bar{y})$  indicates a ball of radius  $\rho$ .

**Remark** This result says that, if  $p^*(t) \in \mathcal{D}_{(\bar{x}, \bar{y})}$  for all  $t \geq 0$ , then the average position  $(\bar{\rho}_x, \bar{\rho}_y)$  asymptotically goes to  $(\bar{x}, \bar{y})$ .

### 2.3.4 Implementation

The HESC set-point generation algorithm follows the steps below:

**FIFO update** Stores a first in first out (FIFO) queue of the last  $m$  distance values received from ARTVA and update it each time new data arrive.

**Direction check** Works a bit differently with respect to its counterpart in the previous algorithm: takes an arithmetic mean of the last  $ck$  valid values found and, after  $dk$  data received, compares the distance value of the last found data with the computed mean. If the new value is greater than the mean, changes sign to the formula that computes the set-point. The choice of computing the mean of  $ck$  values and to wait  $dk$  data before performing the check is due to the fact that the imposed circle-shaped (or eight-shaped, alternatively) trajectory results in consecutive distance values which are not always decreasing, even if the drone is moving in the right direction. Both  $ck$  and  $dk$  are tunable coefficients.

**Yaw correction** Exactly like the previous presented algorithm, computes the yaw correction to be applied to the drone if the angle values received from ARTVA is greater than a certain threshold:

if  $angle\_value > threshold$  then apply the yaw correction

The yaw correction is saturated to a maximum value in such a way to be applied gradually each time a new set-point is given to the controller:

if  $angle\_value \leq yaw\_correction\_max$  then  $yaw\_correction = angle\_value$   
else  $yaw\_correction = yaw\_correction\_max$

In this way, we avoid to have non-consistent consecutive ARTVA measures, which will create difficulties in the data validation phase.

**Jump map velocity computation** Uses the values stored in the FIFO queue to compute the perturbation coefficients:

$$\begin{aligned} w_x &= \frac{1}{m} \sum_{j=1}^m FIFO(j) \sin(j\omega_x) \\ w_y &= \frac{1}{m} \sum_{j=1}^m FIFO(j) \sin(j\omega_y) \end{aligned} \quad (2.56)$$

**Flow map velocity computation** Computes velocity values from perturbation coefficients found in the previous step and velocity values from the last iteration:

$$\begin{aligned} v_x(T) &= -k_{1x}v_x(T-1) - k_{2x}w_x(T) \\ v_y(T) &= -k_{1y}v_y(T-1) - k_{2y}w_y(T) \end{aligned} \quad (2.57)$$

where  $T$  is the period between two ARTVA transmissions. Then, the two obtained velocity values are saturated to a maximum:

$$\begin{aligned} &\text{if } velocity\_value \leq velocity\_max \text{ then } velocity\_set\_point = velocity\_value \\ &\text{else } velocity\_set\_point = velocity\_max \end{aligned}$$

**Position set-point computation** Position set-point values are computed from velocity set-point values. Those values are scaled by a sort of saturation function: the closer the drone is to the beacon transmitter, the lower is the distance between consecutive position set-points. In this way the oscillations are strongly mitigated when the drone is near to the beacon transmitter, avoiding the vehicle to step away from it:

$$\begin{aligned} p_{spx} &= H v_x \\ p_{spx} &= H v_y \end{aligned} \quad (2.58)$$

where  $H$  is the above mentioned mitigation function.

**Reference system transformation** Similarly to the Flux Line algorithm, transforms the reference system from the one in agreement with the body to the inertial one. Furthermore, add to each of the two components the term used to impose the



circle-shaped (or eight-shaped, alternatively) trajectory:

$$\begin{aligned} p_{spX} &= p_{spx} \cdot \cos(\gamma) + p_{spx} \cdot \sin(\gamma) + \rho_x \cdot \cos(\omega_x t) \\ p_{spY} &= -p_{spx} \cdot \sin(\gamma) + p_{spx} \cdot \cos(\gamma) + \rho_y \cdot \sin(\omega_y t) \end{aligned} \quad (2.59)$$

where  $\gamma$  is the residual value of the yaw angle of the drone after the correction.

Finally, the algorithm publishes the two value of the position set-point and the value of the yaw correction to a topic from which the controller can read them.

## 2.4 General control scheme

The general position control scheme of the autopilot module, updated with the presented algorithms for generation of the set-point, is shown in Figure 2.7. The algorithm selection decides which of the two algorithms to run and activates the relative switch. The possible operative configurations are the following:

**Flux Line mode** Switch B is activated (up);

**HESC mode** Switch A is activated and switch B is deactivated (down);

**Standard mode** Both switches are deactivated.

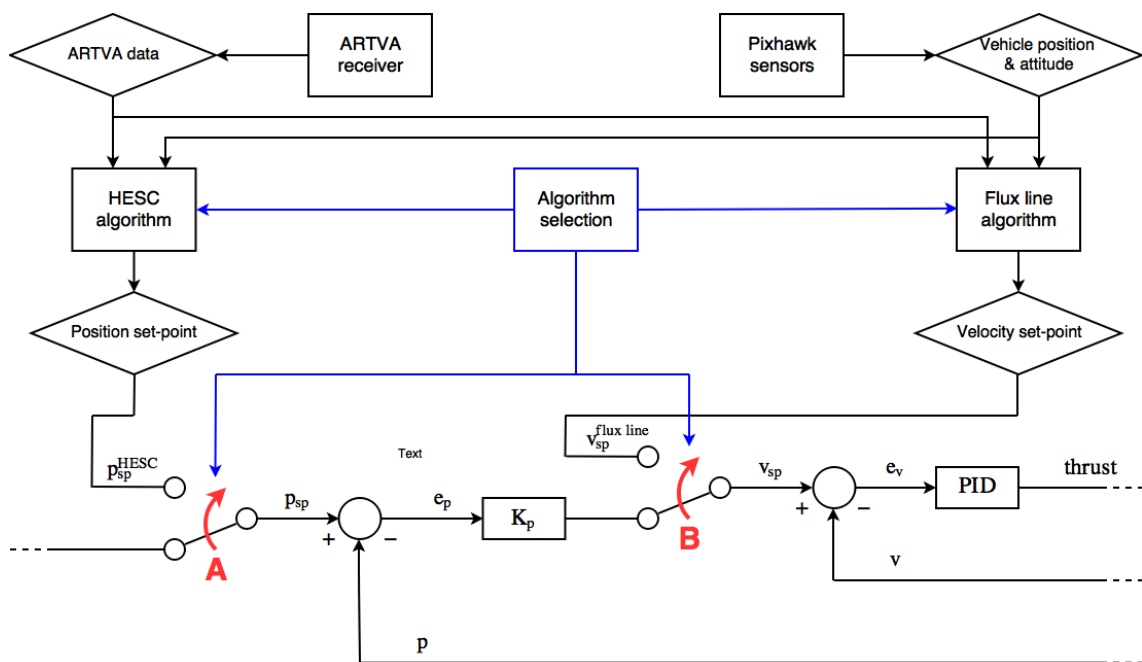


Figure 2.8. General control scheme.

# Chapter 3

## Results

Below we will analyse the results of the simulations of the two presented search algorithms, and the main issues related to the practical implementation of the system.

### 3.1 Simulations

The software used to simulate the two algorithms is Robot Operating System (ROS), the main functionalities of which are discussed in the first appendix. The simulations are realized by means of three different ROS nodes:

**Drone and ARTVA simulator** Simulate both the model of the drone, with its dynamical behaviour, and the ARTVA beacon transmitter. The ARTVA equivalent model[8] is obtained considering the nominal magnetic field generated, represented in (2.3), and the magnetic field intensity described by:

$$\|H\| = \frac{\|m\|}{4\pi\|r\|^3} \sqrt{1 + 3 \cos^2 \Theta} \quad (3.1)$$

where the actual distance to the transmitter is indicated by the vector  $r$ , while  $\Theta \in [0, \pi]$  describes the angle between  $r$  and  $m$ . Given  $r_{min} \in \mathbb{R}_{>0}$  and  $r_{max} \in \mathbb{R}_{>0}$ , with  $r_{min} < r_{max}$ , we can define the three operation zones:

- the outer zone:

$$\mathcal{Z}_o := \{p \in \mathbb{R}^3 : \|p - p_t\| > r_{max}\}$$

- the mid zone:

$$\mathcal{Z}_m := \{p \in \mathbb{R}^3 : r_{min} < \|p - p_t\| \leq r_{max}\}$$

- and the inner zone:

$$\mathcal{Z}_i := \{p \in \mathbb{R}^3 : \|p - p_t\| \leq r_{min}\}$$

where  $p$  and  $p_t$  are the positions of the receiver and the transmitter, respectively. From (2.3), the value of distance  $d$ , output of the receiver, can be approximated in the following way:

$$d = \left( \frac{k_{eq}}{4\pi \|C(\mathcal{R}^T H + w)\|} \right)^{\frac{1}{3}} \quad (3.2)$$

where  $k_{eq}$  is a positive constant,  $\mathcal{R}$  is the receiver orientation, and  $C$  is a selection matrix that assumes two different values,  $C_{P2}$  and  $C_{P3}$ :

$$C_{P2} = [1 \ 0 \ 0]$$

$$C_{P3} = I_{3 \times 3}$$

leading so to two possible distance calculations, namely  $d_{P2}$  and  $d_{P3}$ . The receiver first determines the distance  $d_{P3}$  and, if  $d_{P3} < 300$ , sets the angle  $\delta(k)$  to zero and  $d(k) = d_{P3}$ , otherwise calculates the distance  $d_{P2}$ . If  $d_{P2} < 5000$ , then the receiver determines the  $\delta$  angle by means of the following equation:

$$\delta = \tan^{-1} \left( \frac{[0 \ 1 \ 0](\mathcal{R}^T H + w)}{[1 \ 0 \ 0](\mathcal{R}^T H + w)} \right) \quad (3.3)$$

and imposes  $d(k) = d_{P2}$ . Lastly, if  $d_{P2} > 5000$ , the receiver's output is  $d(k) = -1$  and  $\delta(k) = 0$ . The vector  $w = [w_{bx} \ w_{by} \ w_{bz}]^T$  represents the electromagnetic interferences, expressed in body frame, and can be written as sum of drone noises,  $w_d$ , and environmental noises  $w_e$ .

In the end, both  $d$  and  $\delta$ , obtained from (3.2) and (3.3), are discretised and sampled by means of a standard zero-hold filter to simulate their digital nature.

**Set-point generation algorithm** Contain the implementation of the algorithm (Flux Line or HESC).

**Controller simulator** Simulate a simple discrete integrator.

To perform the simulation, the three nodes has to be run in parallel on three different terminal windows. We will present the results of the simulation of four different cases in which, while the simulated drone is always initially placed at the origin of the inertial reference frame, with the body frame coincident with it, the simulated transmitter is placed in different spots:

- Case A: transmitter at  $(10, 15, -2)$ ;
- Case B: transmitter at  $(-6, 16, -2)$ ;
- Case C: transmitter at  $(-14, -9, -2)$ ;
- Case D: transmitter at  $(12, -13, -2)$ .

The distance unit represents a metre, thus, in each case, the simulated transmitter is more or less 17 metres far from the simulated drone and 2 metres under the snow.

### 3.1.1 Flux Line algorithm simulation

The output positions of the simulated drone, obtained by means of set-points generated with Flux Line search algorithm, and collected at each integration step, are plotted in Figures 3.1-4. The algorithm performs quite well, with the simulated drone going straight toward the transmitter's position and reaching it with a good precision. Once it gets to the minimum distance point, the simulated drone starts moving forward and backward on the same line, remaining in the neighbourhood of the target. This is due to the *direction check* step of the algorithm, which imposes to the vehicle a velocity set-point equal to the last one but with opposite sign each time the drone steps away from the transmitter's position, and to the fact that, when the drone is very close to the transmitter, the received angle value is zero, and so the *yaw correction* step does not intervene, forcing the vehicle to maintain always the same orientation. Moreover, thanks to the saturation of the velocity, the vehicle will move slowly when the detected distance is small, avoiding so to go too far from the target.

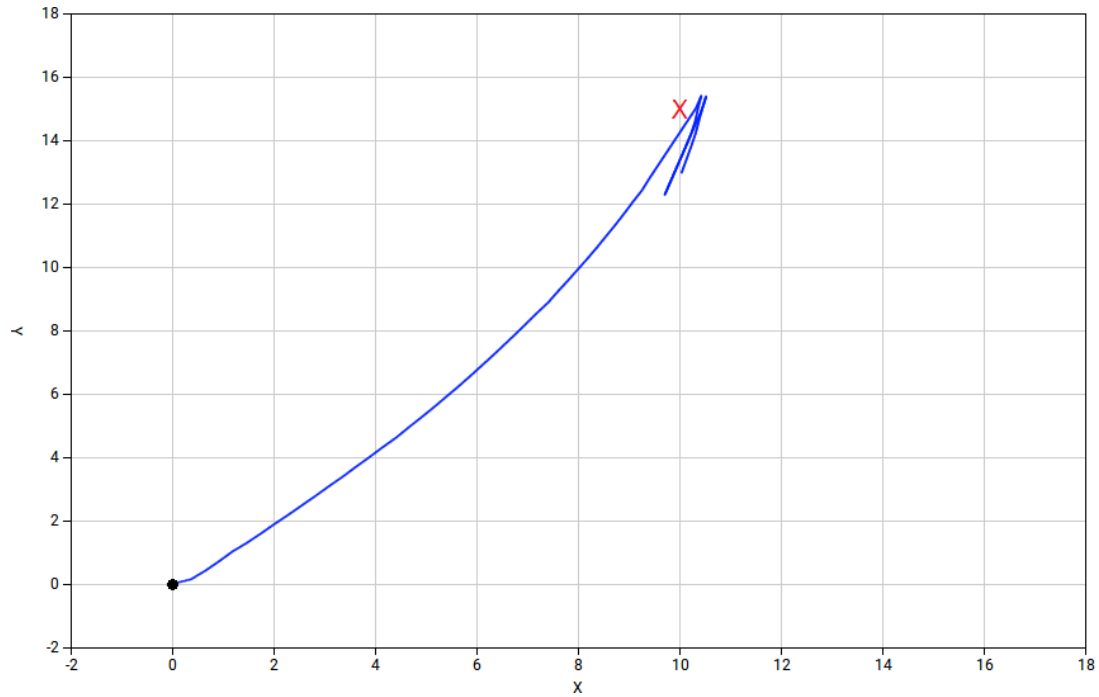


**Figure 3.1.** Flux Line algorithm simulation case A: transmitter at  $(10, 15, -2)$ , the black dot represents the initial position of the drone, the blue line represents the drone trajectory, the red cross represents the transmitter's position.

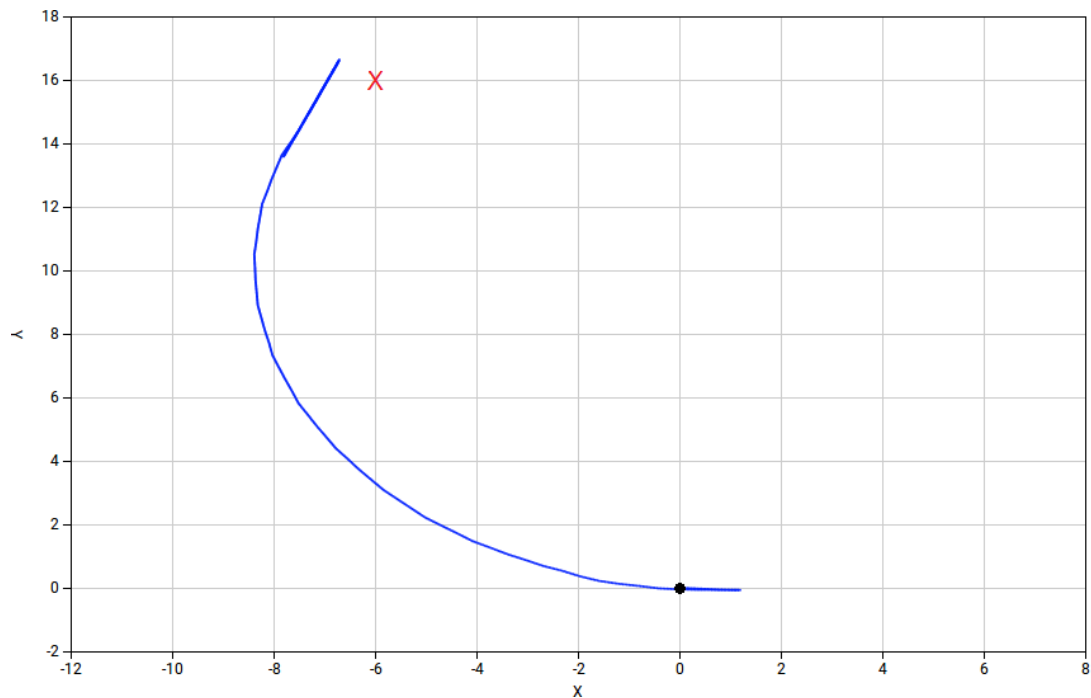


**Figure 3.2.** Flux Line algorithm simulation case B: transmitter at  $(-6, 16, -2)$ , the black dot represents the initial position of the drone, the blue line represents the drone trajectory, the red cross represents the transmitter's position.

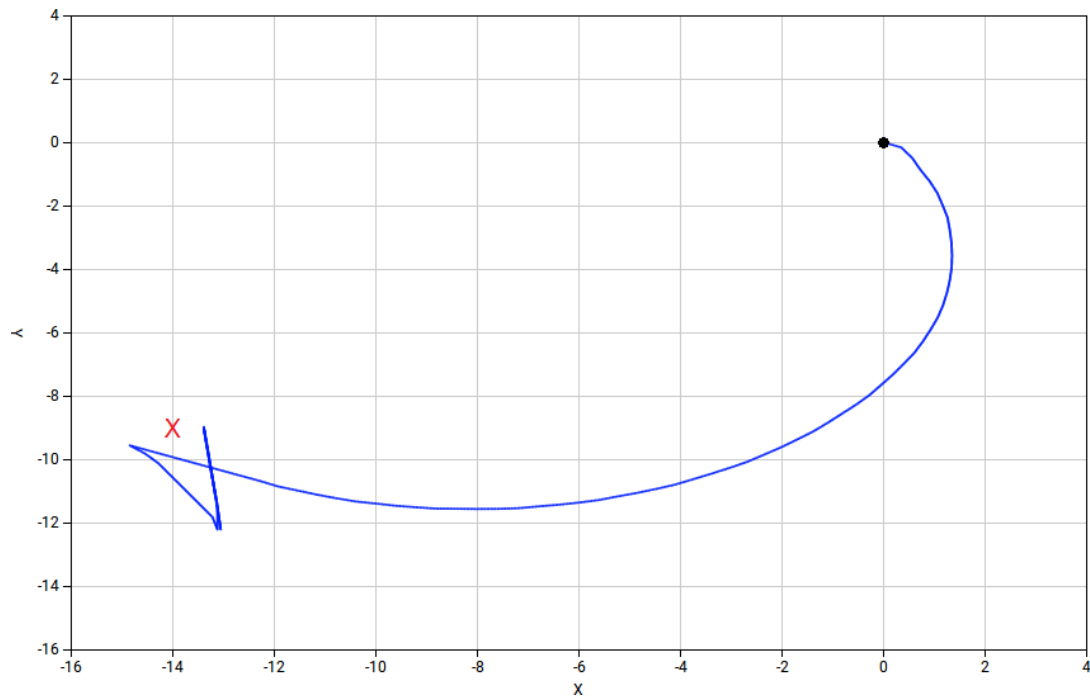


**Figure 3.3.** Flux Line algorithm simulation case C: transmitter at  $(-14, -9, -2)$ , the black dot represents the initial position of the drone, the blue line represents the drone trajectory, the red cross represents the transmitter's position.

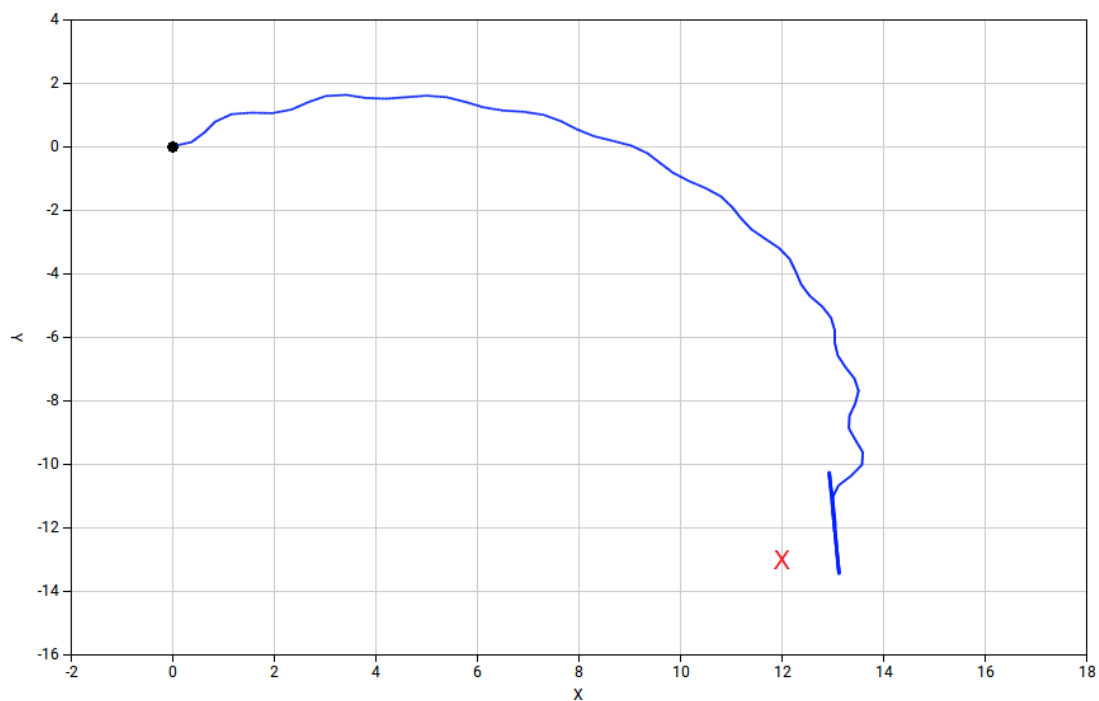


**Figure 3.4.** Flux Line algorithm simulation case D: transmitter at  $(12, -13, -2)$ , the black dot represents the initial position of the drone, the blue line represents the drone trajectory, the red cross represents the transmitter's position.

### 3.1.2 HESC algorithm simulation

Same as before, the output positions of the simulated drone, obtained this time by means of set-points generated with circle-shaped HESC search algorithm and eight-shaped HESC search algorithm, and collected at each integration step, are plotted in Figures 3.5-8 and 3.9-12 respectively. Also this algorithm performs well, with the simulated drone moving toward the transmitter's position with the imposed oscillating movement. The more the vehicle gets closer to the target, the more the trajectory takes the geometry of a series of circles (or a series of eight-shaped paths, alternatively). Once it gets close to the transmitter's position, the drone continues oscillating, remaining in its neighbourhood. This is due to the mitigation function, which reduces the imposed perturbations, and so the velocity of the vehicle, the closer it gets to the target, and to the *direction check* step of the algorithms, which reverses the motion if the drone goes too far from the transmitter's position.

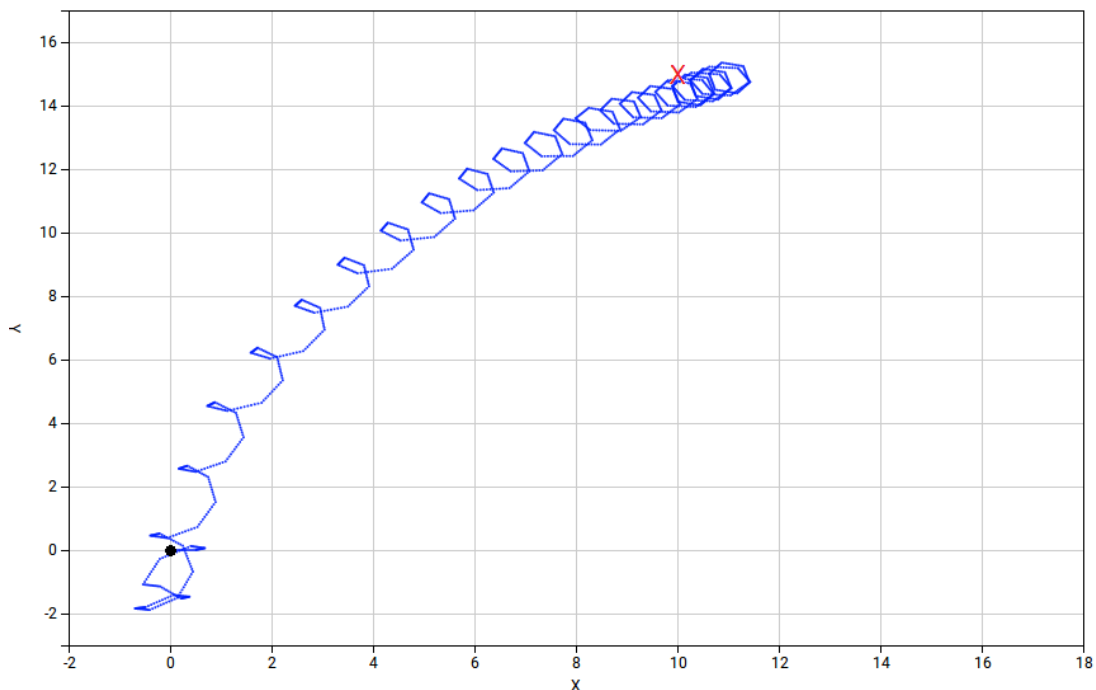


**Figure 3.5.** Circle-shaped HESC algorithm simulation case A: transmitter at  $(10, 15, -2)$ , the black dot represents the initial position of the drone, the blue line represents the drone trajectory, the red cross represents the transmitter's position.



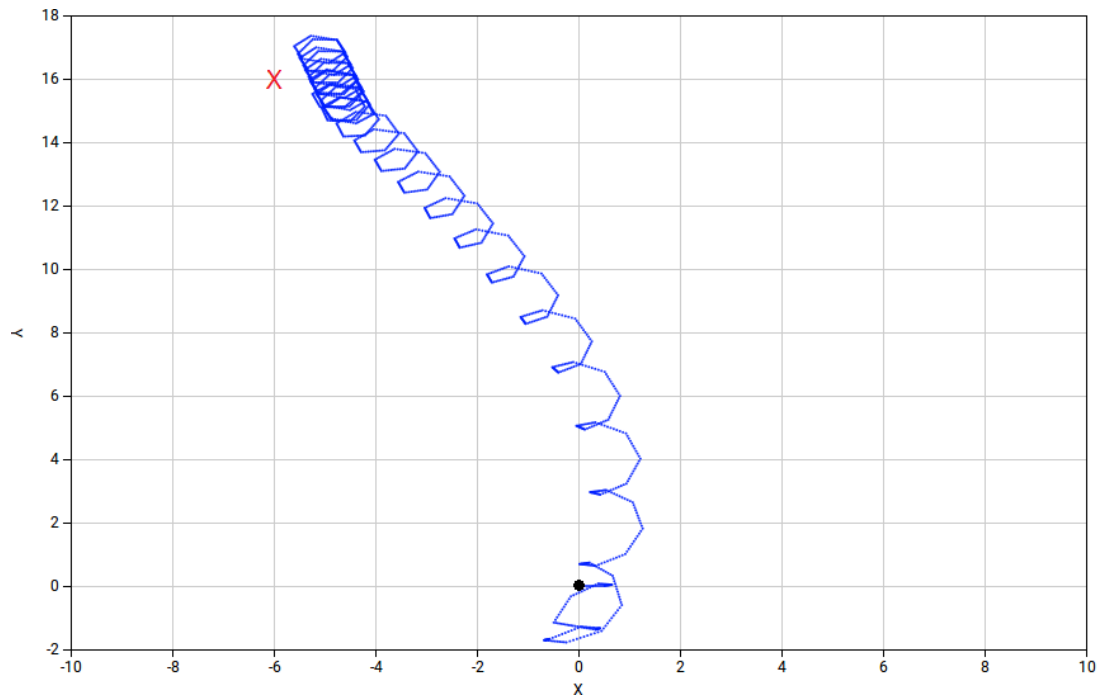


**Figure 3.6.** Circle-shaped HESC algorithm simulation case B: transmitter at  $(-6, 16, -2)$ , the black dot represents the initial position of the drone, the blue line represents the drone trajectory, the red cross represents the transmitter's position.

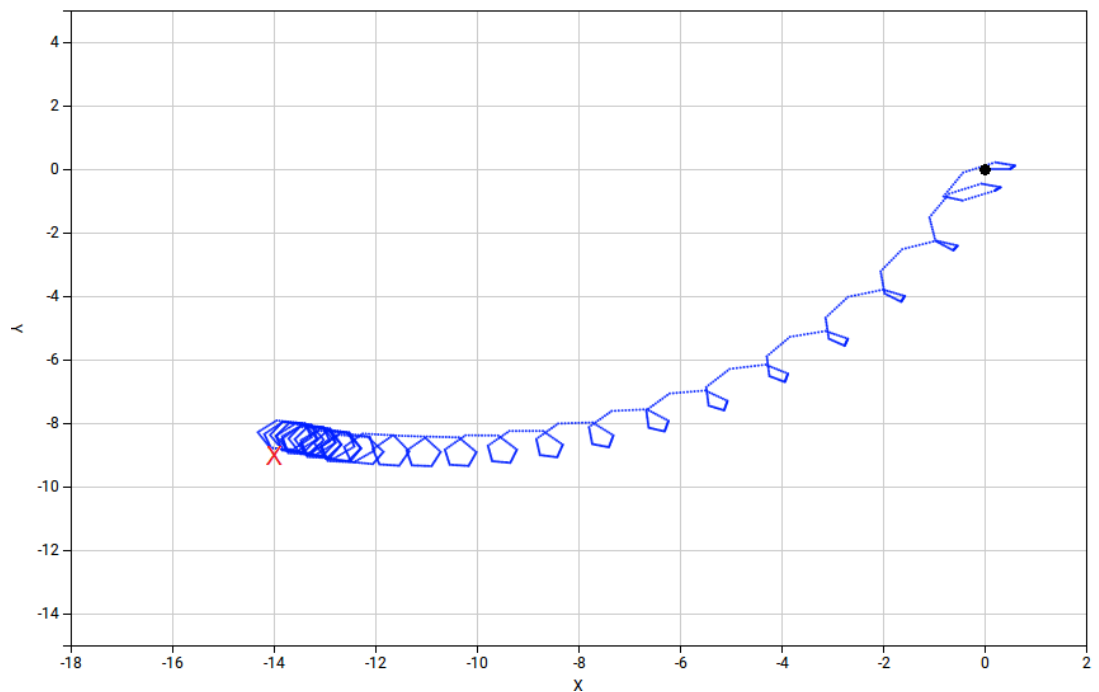


**Figure 3.7.** Circle-shaped HESC algorithm simulation case C: transmitter at  $(-14, -9, -2)$ , the black dot represents the initial position of the drone, the blue line represents the drone trajectory, the red cross represents the transmitter's position.

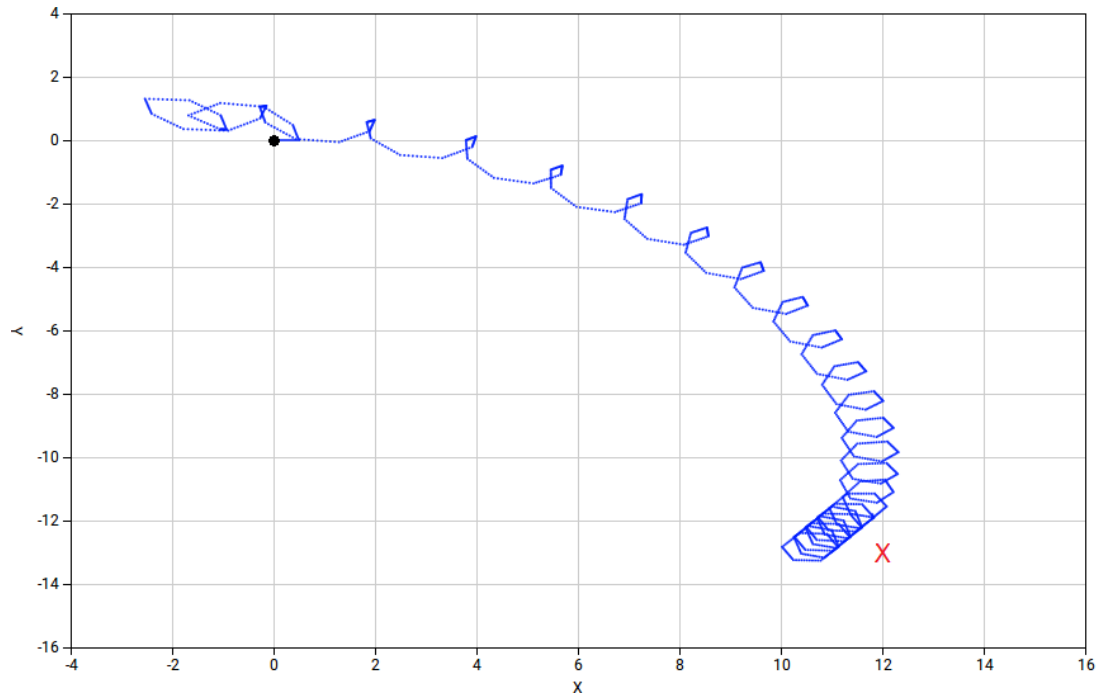


**Figure 3.8.** Circle-shaped HESC algorithm simulation case D: transmitter at  $(12, -13, -2)$ , the black dot represents the initial position of the drone, the blue line represents the drone trajectory, the red cross represents the transmitter's position.

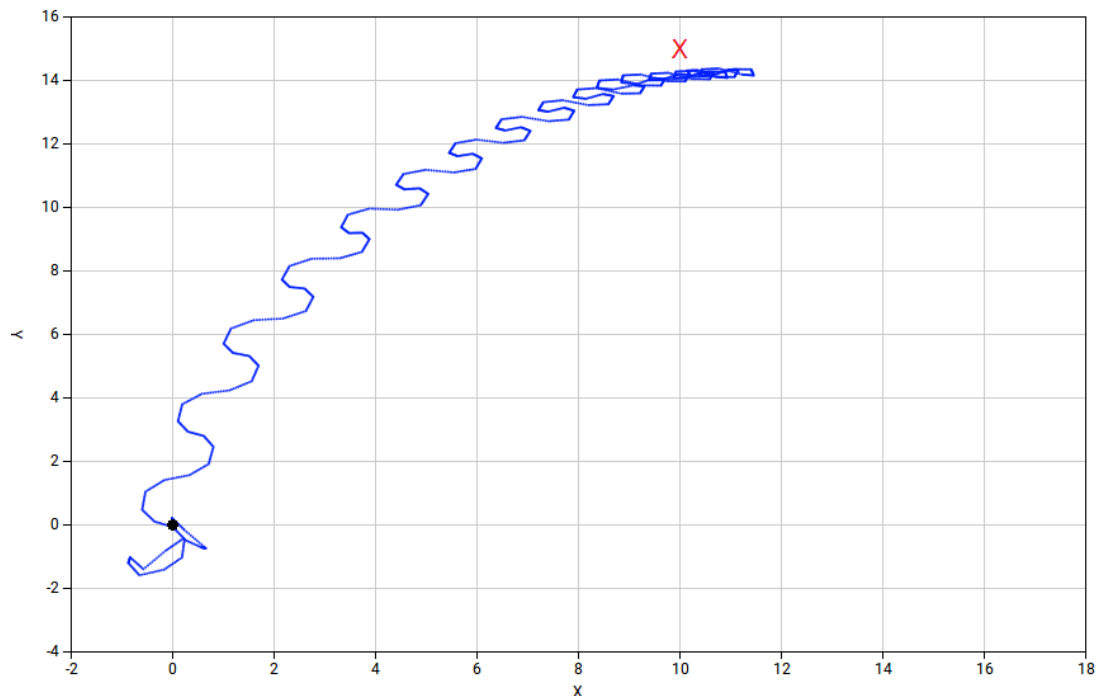


**Figure 3.9.** Eight-shaped HESC algorithm simulation case A: transmitter at  $(10, 15, -2)$ , the black dot represents the initial position of the drone, the blue line represents the drone trajectory, the red cross represents the transmitter's position.

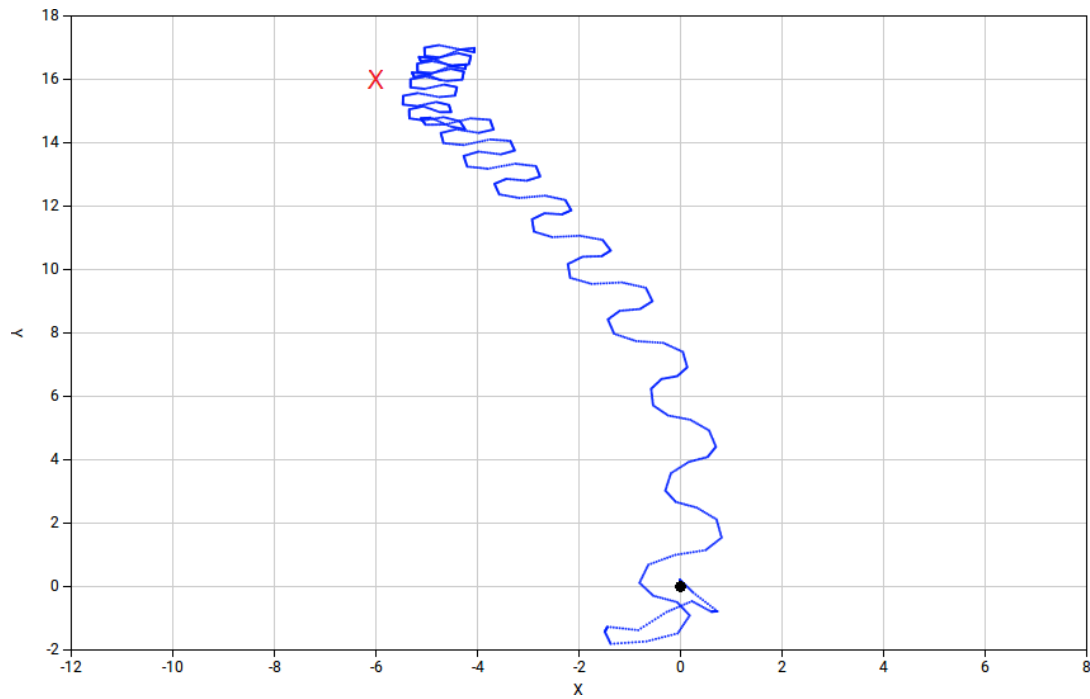


**Figure 3.10.** Eight-shaped HESC algorithm simulation case B: transmitter at  $(-6, 16, -2)$ , the black dot represents the initial position of the drone, the blue line represents the drone trajectory, the red cross represents the transmitter's position.

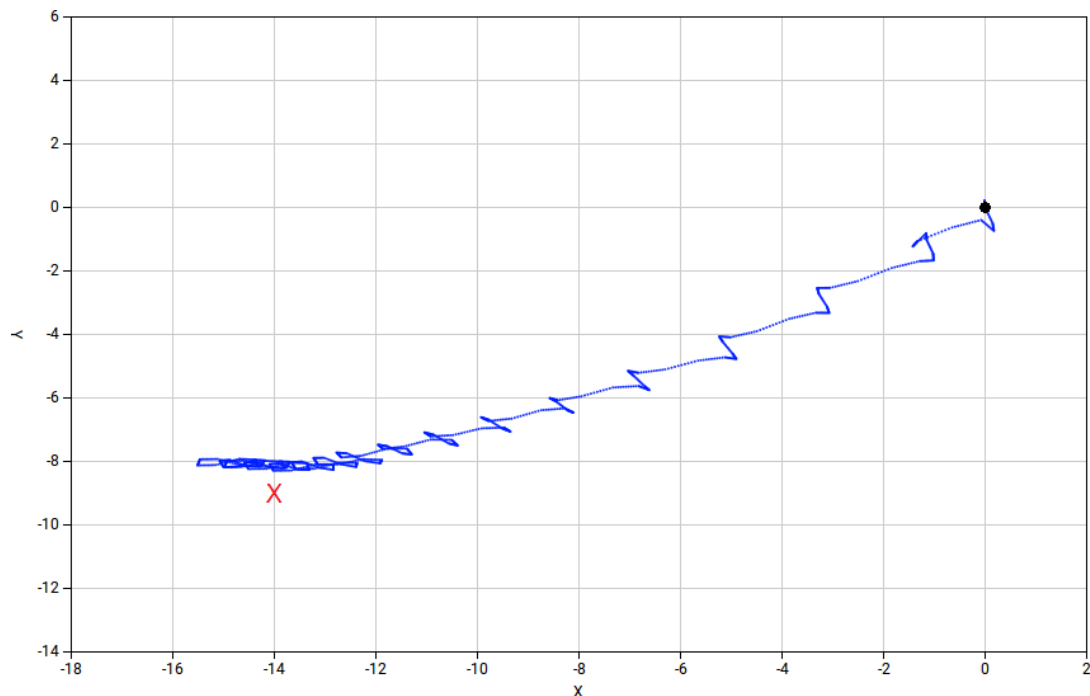


**Figure 3.11.** Eight-shaped HESC algorithm simulation case C: transmitter at  $(-14, -9, -2)$ , the black dot represents the initial position of the drone, the blue line represents the drone trajectory, the red cross represents the transmitter's position.

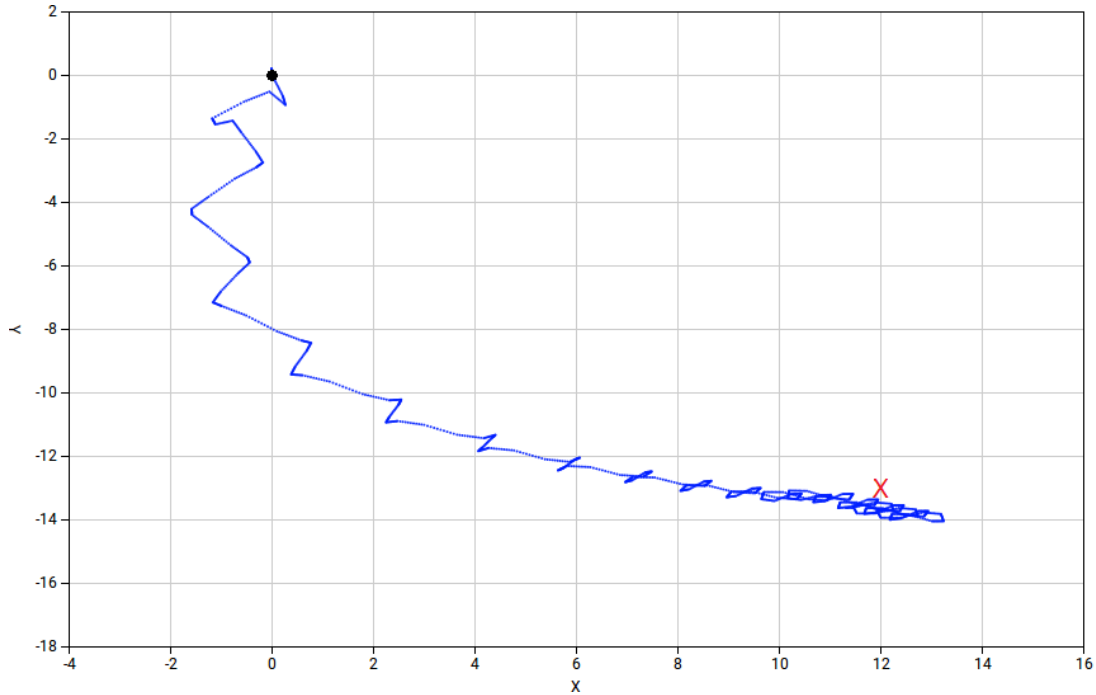


**Figure 3.12.** Eight-shaped HESC algorithm simulation case D: transmitter at  $(12, -13, -2)$ , the black dot represents the initial position of the drone, the blue line represents the drone trajectory, the red cross represents the transmitter's position.

### 3.1.3 Algorithms comparison

Now we will show a comparison between the two new proposed algorithms and the Cross Flight algorithm described in the first chapter of this document, focusing on the time they take to drive the simulated drone to the transmitter's position, in such a way to highlights their performance. For each algorithm, four simulations has been run using the four cases of transmitter's position presented before; the results of those simulations, namely the time each algorithm takes for each single run and the average time, are reported in Table 3.1. The maximum reference velocity imposed for each algorithm is  $2 \text{ m/s}$ . Furthermore, for Flux Line and HESC algorithms the simulation stops as soon as the drone gets close to the transmitter ( $d < 250$ ), while the Cross Flight algorithm simulation stops when it reaches the computed position.

It is straightforward to see that Flux Line and HESC algorithms performs much better than Cross Flight. Moreover, we can state that Flux Line is slightly faster than HESC algorithms, mainly because of the oscillating trajectory of the seconds with respect to the straight one of the first.

Search algorithm	Case A	Case B	Case C	Case D	Average
Flux Line	29.62	33.58	31.59	28.55	30.84
Circle-shaped HESC	45.45	43.45	41.03	46.93	44.22
Eight-shaped HESC	45.39	42.51	42.45	45.35	43.93
Cross Flight	117.54	140.70	114.20	106.16	119.65

**Table 3.1.** Algorithms comparison: the time is expressed in seconds; case A:  $(10, 15, -2)$ , case B:  $(-6, 16, -2)$ , case C:  $(-14, -9, -2)$ , case D:  $(12, -13, -2)$ .

## 3.2 Practical implementation

Regarding the practical implementation, it has been possible to test the operation of the ARTVA system under different conditions. Nevertheless, we are not been able to test the two presented search algorithms, both because some additional control structures are needed, like take-off, landing and altitude management, and because of issues related to ARTVA system implementation.

The main problem is the electromagnetic noise produced by brushless motors and by the modulation technique adopted for the electronic speed controllers (ESCs). These electromagnetic disturbances are low frequency signals, and when their intensity is high enough, the ARTVA receiver sees them, and consequently handles them, as ARTVA transmitter's signals. By carrying out several tests under different conditions, as said before, we have been able to observe the capability of ARTVA system and the behaviour of electromagnetic disturbances. The tests made can be categorized as follows:

- motors off;
- motors on, without shielding;
- motors on, with standard aluminium shielding;
- motors on, with EMI aluminium shielding.

### 3.2.1 Test with motors off

The first test has been taken with motors off, and had the aim to verify the actual range of the ARTVA system. The values of the received distance measures, related to

the actual distance between the transmitter and the receiver, are reported in Table 3.2. We can state that the progression of the ARTVA distance values are quite linear with respect to actual distances, with a couple of exceptions. In particular, the value read at 6 metres is higher than the one read at 8 metres, so it could be a wrong measure, and the range of values read at 12 metres are too high, so they must be some kind of disturbance. Furthermore, it is easy to note that the more is the distance between the transmitter and the receiver, the higher is the variance of the measures obtained at the same distance (e.g. values read at 22 metres). So, we can conclude that the system is reliable within a distance of about 20 metres.

Actual distance (metres)	ARTVA distance value
0	53
2	425
4	545
6	746
8	729
10	805
12	1838 / 1974
14	1036 / 1053
16	1242 / 1276
18	1648 / 1674
20	2140 / 2200
22	2140 / 2701

**Table 3.2.** Test results: motors off.

### 3.2.2 Test with motors on and no shielding

Another test has been taken with motors on, without propellers and with a constant throttle of about 25%, so to verify the effect of the magnetic disturbances on the measure. The results are reported in Table 3.3. It is immediate to see that with motors on we have a drastic decrease in the quality of the measurement. Indeed, at distance greater than

6 metres, the ARTVA values we read are influenced by electromagnetic noises. This is highlighted by the fact that from 8 metres up, the received value is always the same.

Actual distance (metres)	ARTVA distance value
0	50
2	272
4	506
6	638
8	849
10	849

**Table 3.3.** Test results: motors on, no shielding.

### 3.2.3 Test with motors on and standard aluminium shielding

Since our aim is to be able to use the entire 20 metres range within which the ARTVA measurements are reliable, we have tried to solve this problem by isolating the motors housings and the drone's arms, which contain the ESCs, with standard aluminium tape, aiming to contain the electromagnetic interferences. Then we repeated the test, the results of which are reported in Table 3.4. This solution is not working, since we have not increased the range of valid measurements with respect to the previous test.

Actual distance (metres)	ARTVA distance value
2	289
4	459
6	535
8	700
10	700

**Table 3.4.** Test results: motors on, standard aluminium shielding.

### 3.2.4 Test with motors on and EMI aluminium shielding

Finally, we have tried to repeat the isolation solution using an electromagnetic interference (EMI) shielding aluminium tape, instead of a standard one. So we have isolated the motors housings and the drone's arms with the EMI aluminium tape, and then we have repeated the test. The results are shown in Table 3.5. We have obtained just a slight improvement in the quality of the measure (about 2 metres), which is absolutely not enough for our purposes. This suggests that, despite the total isolation, there is still an escape route for electromagnetic disturbances.

Actual distance (metres)	ARTVA distance value
2	343
4	506
6	545
8	621
10	700
12	700

**Table 3.5.** Test results: motors on, EMI aluminium shielding.



# Conclusions

Avalanche beacon systems are very helpful devices for the intent of saving people buried under snow due to avalanches. Their implementation on aerial robots can lead to even better results, speeding up search operations, ensuring so a faster human intervention and raising the chances of finding missing people still alive and in non-critical conditions.

In this thesis, we have analysed two search algorithms, based on the data received by the avalanche beacon transmitter, aiming to improve the search time even more. The innovation proposed by these two algorithms, with respect to the ones that have been proposed until now, is that, as soon as the beacon signal is caught, the quad-copter drone is guided directly toward the victim. From simulations performed with ROS, we observed that both the proposed algorithms performs quite well, leading the drone straight toward the signal source, and making it remain in the neighbourhood of the ARTVA transmitter once find it.

Nevertheless, we have stumbled in some problems which arise with the practical implementation of this system. In particular, the electromagnetic noises coming from motors and ESCs mounted on the quad-copter. These disturbances heavily influence the measures received from ARTVA, significantly decreasing the reliability of the system. As a consequence of this, only the measures obtained around a few metres from the beacon transmitter are correct, while, beyond a certain threshold, all the read values are indeed influenced by the electromagnetic noise. In this way, the efficiency of the presented search algorithms is nullified, since we need to get very close to the ARTVA transmitter in order to get a useful measure. We have tried to handle this issue by isolating the disturbance generating components with a standard aluminium tape first, and then with a EMI aluminium tape, unfortunately obtaining unsatisfactory results.

A possible future development to make the algorithms usable is to change the mechanical configuration of the quad-copter drone; e.g. moving the motors and the ESCs in a central aluminium housing, positioning the motors in such a way that the rotating axes are horizontal, and transmitting the motion to the propellers by means of shafts supported by spherical bearings, mounted inside the drone's arms, at the end of which are placed spiral bevel gears, in such a way to turn by 90 degrees the direction of the rotating axes.

# Appendix A

## First Appendix

Here are reported the description of some basis concepts, software structures and tools that have been used in the project.

### A.1 PX4

PX4 is the software running on the Pixhawk autopilot module. It consists in two main layers[9]: the flight stack, which is an estimation and flight control system, and the middleware, which is a general robotics layer that can support any type of autonomous robot, providing internal/external communications and hardware integration. Modules communicate with each other through a publish-subscribe message bus named uORB. PX4 code runs on a real-time operating system (RTOS) named NuttX.

#### A.1.1 Flight stack

The flight stack is a collection of guidance, navigation and control algorithms for autonomous drones. Figure A.1 shows an overview of the building blocks of the flight stack. The estimator takes one or more sensor inputs and combines them to compute a vehicle state. The controller takes a set-point and a measurement or estimated state as input and adjust the value of the process variable such that it matches the set-point; the output is a correction to eventually reach that set-point. The mixer takes force commands and translates them into individual motor commands, while ensuring that some limits are not exceeded.

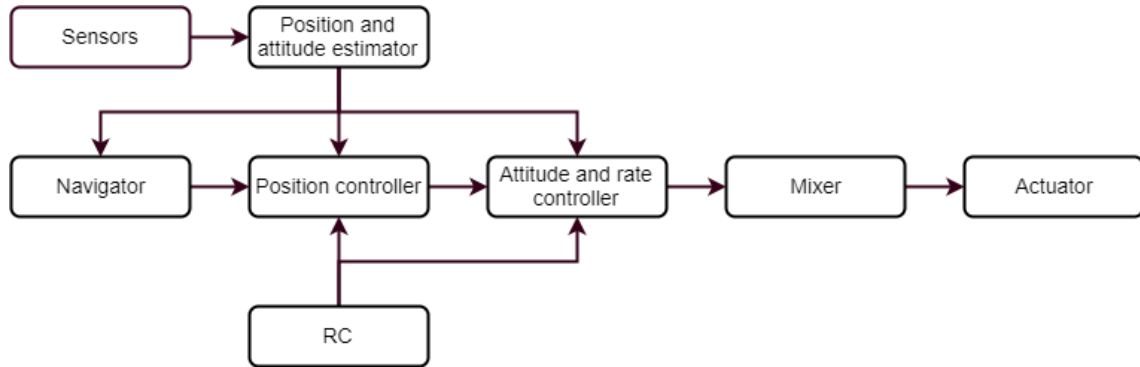


**Figure A.1.** Flight stack architecture.

### A.1.2 Middleware

The middleware consists primarily of device drivers for embedded sensors, communication with the external world, and the uORB publish/subscribe message bus. In addition, the middleware includes a simulation layer that allows PX4 flight code to run on a desktop operating system and control a computer modelled vehicle in a simulated world.

### A.1.3 NuttX

NuttX is the RTOS on which the PX4 code runs, and it is open source, light-weight, efficient and very stable. Modules are executed as tasks, namely each of them has its own file descriptor list, but they share a single address space. A task can still start one or more threads that share the file descriptor list. Each task or thread has a fixed-size stack, and there is a periodic task which checks that all stacks have enough free space left.

## A.2 Communication over serial port

In order to make individual circuits to exchange information, they must share a common communication protocol[10]. Among all existent protocols, we can distinguish two main categories: parallel and serial. The main difference between parallel and serial protocols is that parallel ones can transfer multiple bits at the same time, using buses of data made of several wires; serial ones, instead, stream their data one single bit at a

time, requiring a reduced number of wires, sometimes just one. In conclusion, parallel communication is certainly faster and easier to implement, but requires many more input/output lines, while serial communication is slower but cheaper in terms of space and wires.

In Figures A.2 and A.3 are represented an example of parallel communication and one of serial communication, respectively. For our purpose of transmitting data from ARTVA receiver to Pixhawk, we opt to use one of the five serial communication ports which are embedded in the board.

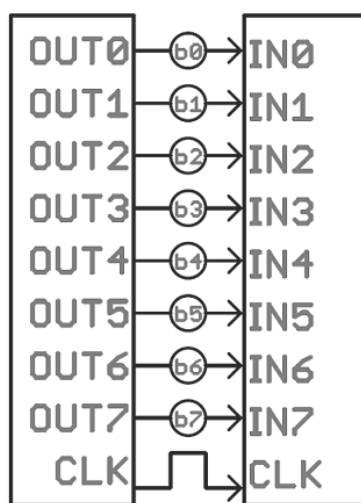


**Figure A.2.** Example of parallel interface: an 8-bit data bus, controlled by a clock, transmitting a byte every clock pulse. 9 wires are used.

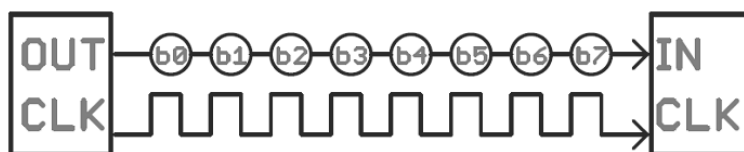


**Figure A.3.** Example of serial interface: a single bit is transmitted every clock pulse. Just 2 wires are used.

### A.2.1 Asynchronous serial protocol

Serial communication protocols could be subdivided in two groups: synchronous and asynchronous. In a synchronous serial communication, data lines are always paired with

a clock signal in such a way that all connected devices shares the same clock. This will result in a more straightforward and faster transmission, but it requires at least an extra wire between communicating devices. Conversely, asynchronous serial communications does not need the support of an external clock, minimizing so the required wires, but requiring more effort in ensuring the reliability of the transferring and receiving data. The protocol that we use for our purpose is the most common form of asynchronous serial communication.

### A.2.2 Rules of serial communication

The asynchronous serial communication protocol presents a series of mechanisms with specific rules, which help ensuring robust and error-free data transfers, compensating the lack of the external clock. These mechanisms are:

- data bits,
- synchronization bits,
- parity bits,
- and baud rate.

The protocol is highly configurable and there are several way to transfer data serially; the critical part is to ensure that both the communicating devices are configured to use the exact same protocol.

**Data block** The data block contains the information carried by the serial packet. A single packet can be set to contain from 5 to 9 bits of data. The standard data size is the basic 8-bit byte. Other than on the single character-length, the two connected device must agree also on the endianness of the data. In big-endian the most significant byte, namely the one containing the most significant bit, is stored or sent first, and then the following bytes are stored or sent in decreasing significant order; vice versa in little-endian.

**Synchronization bits** The synchronization bits are special kind of bits, a start bit and one or two stop bits, which are used to mark, as their names suggest, at the beginning and at the end of the packet respectively.

**Parity bits** Parity is a simple method used for error checking. It could assume two values: even or odd. To produce the parity bit, all the bits of the data byte are added up, and the evenness of the sum decides whether the bit is set or not. Parity is optional and rarely used.

**Framing the data** The information transmitted is sent in a frame of bits. A data frame is composed by the data block, which is usually one byte, the synchronization bits and, eventually, the parity bit. Figure A.4 represents a data frame.



**Figure A.4.** Example of a serial data frame.

**Baud rate** The baud rate, expressed in unity of bits-per-second, specify how fast the data is sent over a serial line. In order to communicate, two devices must operate at the same baud rate. The higher the baud rate is, the faster the data is transferred, but there are limits due to the clocks and sampling periods of the connected devices.

**8-N-1 9600** The acronym 8-N-1 9600 stands for: 8 data bits, no parity bit, 1 stop beat, and 9600 bps baud rate. This is one of the most commonly used serial data format, and it is the one used for the communication between the ARTVA receiver and Pixhawk.

## A.3 Publish/subscribe structure

Publish/subscribe is a commonly used messaging structure in software architecture based on the fact that the sender, called publisher, do not communicate directly to a receiver, called subscriber, but, instead, publish messages into a topic without having the knowledge of what and how many subscriber, if any, are interested in receiving those messages.

As said before in this appendix, PX4 software, running on Pixhawk autopilot module, predisposes uORB[9]: an asynchronous publish/subscribe messaging application programming interface (API) used for inter-threads/inter-processes communication. uORB

is automatically started when the PX4 software is executed, since many applications depend on it.

The main elements of the uORB messaging API are:

- topic,
- publisher,
- subscriber.

Below it is described how to enable uORB messaging between PX4 modules.

### A.3.1 Adding a new topic

To add a new topic, it is sufficient to create a *.msg* file, containing the variables that we want to pass from a module to another, inside the */msg* directory of the PX4 software, and add the *.msg* file name to the list present in the file *msg/Cmakelist.txt*, which is also present in the */msg* directory. This procedure will automatically generate the topic at build time, which will be placed in the */uORB/topics* directory and has the form of a structure. To use a topic in a PX4 module, it is necessary to include the following header:

```
#include <uORB/topics/topic_name.h>
```

### A.3.2 Publish into a topic

To publish a message into a topic from a PX4 module, after having included the topic header to the module as shown above, the first thing to do is to declare the publisher variable, which is used just to advertise the topic, and the structure to publish into the topic:

```
orb_advert_t topic_name_pub;  
struct topic_name_s topic_data;
```

Then it is necessary to advertise the topic:

```
topic_name_pub = orb_advertise(ORB_ID(topic_name), &topic_data);
```



Finally, it is possible to publish the variable of the structure into the topic at any point of the execution of the module by means of the following code string:

```
orb_publish(ORB_ID(topic_name), topic_name_pub, &topic_data);
```

After that, the variables are saved into the topic and could be used into another module by subscribing it to that topic.

### A.3.3 Subscribe to a topic

To make a PX4 module subscribe to a topic, in order to take values provided or computed by another module, after having included the topic header, we have to declare the subscriber variable, which is used to subscribe to the topic, the structure in which we want to save the variables taken from the topic, and a boolean variable used to check if the topic has been updated since last time it was checked:

```
int topic_name_sub;  
struct topic_name_s topic_data;  
bool updated;
```

Then we must subscribe to the topic:

```
topic_name_sub = orb_subscribe(ORB_ID(topic_name));
```

Lastly, it is possible, at any point of the execution of the module, to check if other modules have updated the topic variables, and in case they have, to make a copy of the updated variables by executing the strings of code shown below:

```
orb_check(topic_name_sub, &updated);  
if (updated) orb_copy(ORB_ID(topic_name), topic_name_sub, &topic_data);
```

This will save a copy of the topic variables into the subscriber module, which can use them for its purposes.

## A.4 ROS

Robot Operating System (ROS)[11] is a collection of tools, libraries, and conventions which have the purpose to simplify the creation of complex and robust robot behaviour across a wide variety of platforms. ROS provides a workspace in which are located packages, which can contain nodes, topics, messages, and so on. Below we will analyse some basic functions.

### A.4.1 Creating a package

It is possible to create a package in the “catkin” workspace, inside the */src* folder, using the following script on a terminal:

```
cd ~/catkin_ws/src
catkin_create_pkg new_package std_msgs rospy roscpp
```

where *std\_msgs*, *rospy*, and *roscpp* are the dependencies of the package. This will create a *new\_package* folder which contains a *package.xml* and a *Cmakelist.txt* file, which have been partially filled out with the information we gave in the command (e.g. the dependencies).

### A.4.2 Building the workspace and sourcing the setup file

To build the catkin workspace we have to execute the following command:

```
cd ~/catkin_ws/src
catkin_make
```

After the workspace has been built, it has created a similar structure in the */devel* subfolder. To add the workspace to our ROS environment, we need to source the generated setup file executing the following string:

```
cd ~/catkin_ws/devel/setup.bash
```

### A.4.3 ROS nodes

A node is an executable file within a ROS package. ROS nodes use a ROS client library to communicate with other nodes. Moreover, nodes can publish or subscribe to a topic and can also provide or use a service. To display information about ROS nodes that are currently running we can use the following command:

```
rostopic list
```

Furthermore, if we want information about a specific node, we can run the following command:

```
rostopic info /node_name
```

To directly run a node within a package, without having to know the package path, we have just to run the following string:

```
roslaunch [package_name] [node_name]
```

### A.4.4 ROS topics

Topics are created from *.msg* files during the execution of ROS environment and are automatically destroyed when the execution is stopped. In order to get information about ROS topics currently subscribed to and published, we can run the following command:

```
rostopic list
```

To show the data published on a topic, we have to run the following string:

```
rostopic echo [topic_name]
```

### A.4.5 Launch a ROS node with a launch file

A launch file, located in the */launch* folder of a package, serves to run a node with specific dependencies. To start a node as defined in a launch file we can use the following command:

```
roslaunch [package_name] [launchfile_name.launch]
```



# Appendix B

## Second Appendix

Here is reported the code used to realize the interfacing between the ARTVA system and Pixhawk autopilot module, and to implement the search algorithms.

### B.1 ARTVA system interfacing

Below is shown the code of the reading function and the validation algorithm.

#### B.1.1 Reading ARTVA data

Read the message

```
int read_port() {  
  
    int i = 1;  
    int n = 0;  
    char temp_buf = '\0';  
  
    // Clean up the message array before start reading  
    memset(artva_msg, '\0', sizeof artva_msg);  
  
    // Start the reading cycle  
    while (temp_buf != 0xDE) {  
        read(fd, &temp_buf, 1);  
        temp_buf -= 0x55;  
    }  
}
```

```
n = 1;
artva_msg[0] = temp_buf;
while (i < 32) {
    n = read(fd, &temp_buf, 1);
    temp_buf -= 0x55;
    artva_msg[i] = temp_buf;
    i += n;
}

return 0;
}
```

### Validity check

```
int check_ARTVA() {

    msg_val = true;

    //Check if the header is valid
    if (artva_msg[0] != 0xDE) msg_val = false;
    if (artva_msg[1] != 0xFA) msg_val = false;
    if (artva_msg[2] != 0xBE) msg_val = false;
    if (artva_msg[3] != 0xBA) msg_val = false;

    //Check if the footer is valid
    if (artva_msg[28] != 0xAB) msg_val = false;
    if (artva_msg[29] != 0xEB) msg_val = false;
    if (artva_msg[30] != 0xAF) msg_val = false;
    if (artva_msg[31] != 0xED) msg_val = false;

    return 0;
}
```

### Message parsing

```
int parse_ARTVA() {

    //Parse the message (little-endian)
    uint16_t d0ne = 0;
```

```
dOne = (uint16_t)((artva_msg[5] << 8) & 0xFF00);
dOne += (uint8_t)((artva_msg[4]) & 0xFF);
sens.d1 = dOne;

uint16_t aOne = 0;
aOne = (int16_t)((artva_msg[7] << 8) & 0xFF00);
aOne += (uint8_t)((artva_msg[6]) & 0xFF);
sens.a1 = aOne;

uint16_t dTwo = 0;
dTwo = (uint16_t)((artva_msg[9] << 8) & 0xFF00);
dTwo += (uint8_t)((artva_msg[8]) & 0xFF);
sens.d2 = dTwo;

uint16_t aTwo = 0;
aTwo = (int16_t)((artva_msg[11] << 8) & 0xFF00);
aTwo += (uint8_t)((artva_msg[10]) & 0xFF);
sens.a2 = aTwo;

uint16_t dThree = 0;
dThree = (uint16_t)((artva_msg[13] << 8) & 0xFF00);
dThree += (uint8_t)((artva_msg[12]) & 0xFF);
sens.d3 = dThree;

uint16_t aThree = 0;
aThree = (int16_t)((artva_msg[15] << 8) & 0xFF00);
aThree += (uint8_t)((artva_msg[14]) & 0xFF);
sens.a3 = aThree;

uint16_t dFour = 0;
dFour = (uint16_t)((artva_msg[17] << 8) & 0xFF00);
dFour += (uint8_t)((artva_msg[16]) & 0xFF);
sens.d4 = dFour;

uint16_t aFour = 0;
aFour = (int16_t)((artva_msg[19] << 8) & 0xFF00);
aFour += (uint8_t)((artva_msg[18]) & 0xFF);
sens.a4 = aFour;
```

```
    sens.tx_det = (artva_msg[20]) & 0xFF;
    sens.tx_count = (artva_msg[21]) & 0xFF;

    return 0;
}
```

## B.1.2 Data validation algorithm

### Parsing data

```
int parse_data() {

    check_artva_topic();
    check_yaw_topic();

    // Determine the transmitter in use
    if (sensor.d1 < threshold && sensor.d1 > 0) {
        d_sample = sensor.d1;
        a_sample = sensor.a1;
        printf("Transmitter #1 detected.\n");
    }
    else if (sensor.d2 < threshold && sensor.d2 > 0) {
        d_sample = sensor.d2;
        a_sample = sensor.a2;
        printf("Transmitter #2 detected.\n");
    }
    else if (sensor.d3 < threshold && sensor.d3 > 0) {
        d_sample = sensor.d3;
        a_sample = sensor.a3;
        printf("Transmitter #3 detected.\n");
    }
    else if (sensor.d4 < threshold && sensor.d4 > 0) {
        d_sample = sensor.d4;
        a_sample = sensor.a4;
        printf("Transmitter #4 detected.\n");
    }
    else {
        d_sample = 65535;
        a_sample = 0;
    }
}
```



```
        printf("No transmitter detected.\n");
    }

    // Update yaw value
    yaw = pos.yaw;

    // Define validity ranges
    d_range = d_sample * 0.5;
    a_range = d_sample * 0.05;

    return 0;
}
```

### First validation

```
int first_validation() {

    while (first_val == false) {
        parse_data();
        d_ref = d_sample;
        a_ref = a_sample;
        int n = 1;

        while (n > 0 && n < fk) {
            parse_data();

            // Consider the angle always positive for the check
            if (a_ref >= 0) a_pos_ref = a_ref;
            else if (a_ref < 0) a_pos_ref = - a_ref;
            if (a_sample >= 0) a_pos_sample = a_sample;
            else if (a_sample < 0) a_pos_sample = - a_sample;

            // Check the validity of the new data
            if (((d_sample < d_ref + d_range)
                && (d_sample > d_ref - d_range)
                && (a_pos_sample < a_pos_ref + a_range)
                && (a_pos_sample > a_pos_ref - a_range)
                && (d_sample < threshold))
                || ((d_sample < 300) && (a_sample == 0))) {
```

```

        // Data have passed the check, let's
        // increment the counter of consecutive good samples
        d_ref = d_sample;
        a_ref = a_sample;
        n++;
    }
    else {
        // Data have not passed the check,
        // let's restart the procedure
        printf("After %d consecutive valid messages,
an invalid one has been found.\n"
"The first validation has to be restarted.\n", n);
        n = 0;
        return 0;
    }
}

d_check = d_sample;
step_val = true;
first_val = true;
hesc_init();
printf("%d consecutive valid messages have been found.\n"
"First validation passed.\n", n);
}

return 0;
}

```

### Step validation

```

int step_validation() {

    parse_data();

    // Check the validity of the new data
    if (((d_sample < d_ref + d_range) && (d_sample > d_ref - d_range)
&& (d_sample < 65535)) || ((d_sample < 300) && (a_sample == 0))) {
        // Data have passed the check and
        // can be used to compute the set-point
    }
}

```

```
d_ref = d_sample;
a_ref = a_sample;
last_val = true;
printf("Valid message found.
It can be used to compute the set-point.\n");
}
else {
    // Data have not passed the check,
    // let's parse some other samples
    int n = 1;
    valid = false;
    sp.p_rx = 0;
    sp.p_ry = 0;
    sp.v_rx = 0;
    sp.v_ry = 0;
    sp.gamma = 0;
    sp.vref_mode = 0;
    sp.hesc_mode = 0;
    orb_publish(ORB_ID(sp_data), sp_topic_pub, &sp);
    printf("A non valid message has been found.
Check the next message.\n");

    while (valid == false) {
        parse_data();

        // Check the validity of the new data
        if (((d_sample < d_ref + d_range)
        && (d_sample > d_ref - d_range) && (d_sample < 65535))
        || ((d_sample < 300) && (a_sample == 0))) {
            // Data have passed the check and
            // can be used to compute the set-point
            d_ref = d_sample;
            a_ref = a_sample;
            last_val = true;
            valid = true;
            printf("Valid message found.
It can be used to compute the set-point.\n");
        }
        else {
```

```

        n++;
        printf("Another consecutive non valid
message has been found.\n");
        if (n == sk) {
            // Too many wrong samples, the procedure
            // will be restarted from the first validation
            first_val = false;
            step_val = false;
            last_val = false;
            valid = true;
            printf("%d consecutive non valid
messages have been found.\n"
"The first validation must be repeated.\n", n);
        }
    }
}

return 0;
}

```

## B.2 Algorithms implementation

Below is shown the code implementation of the two search algorithm.

### B.2.1 Flux Line algorithm

```

int vref_gen() {

    v_r0 = v_max * (d_ref / (sqrt(1 + pow(kd * d_ref, 2))));
    theta = a_ref * M_PI / 180;
    sp.gamma = 0;

    // Direction check
    printf("Check value: %d\n", d_check);
    i++;
    if (i == ck) {
        if (d_sample > d_check) {

```

```
        printf("Change direction!\n");
        sign = - sign;
        change_sign = true;
    }
    d_check = d_sample;
    i = 0;
}

// Yaw correction
if (a_ref < 6 && a_ref > -6) sp.gamma += 0;
else {
    gamma_r0 = - gamma_max * (theta /
        (sqrt(1 + pow(ka * theta, 2))));
    sp.gamma += gamma_r0;
    theta = 0;
}

// Velocity set-point computation in body frame
if (change_sign == true) {
    v_rx = - v_rx;
    v_ry = - v_ry;
}
else {
    v_rx = sign * v_r0 * cos(theta);
    v_ry = sign * v_r0 * sin(theta);
}

// Reference system transformation from body to hearth frame (NED)
sp.v_rx = v_rx * cos(yaw+sp.gamma) + v_ry * sin(yaw+sp.gamma);
sp.v_ry = - v_rx * sin(yaw+sp.gamma) + v_ry * cos(yaw+sp.gamma);
sp.vref_mode = 1;
orb_publish(ORB_ID(sp_data), sp_topic_pub, &sp);
change_sign = false;

return 0;
}
```

## B.2.2 HESC algorithm

```

int hesc_pos_gen() {

    // FIFO update
    int j = 0;
    for (j = 0; j < m; j++) ARTVA_FIFO[m - j - 1] = ARTVA_FIFO[m - j - 2];
    ARTVA_FIFO[0] = d_ref;

    j = 0;
    int k = 0;
    theta = a_ref * M_PI / 180;
    sp.gamma = 0;

    // Direction check
    if (i < ck) d_check += d_sample;
    if (i == dk) {
        d_check = d_check / ck;
        printf("Check value: %d\n", d_check);
        if (d_sample > d_check) {
            printf("Change direction!\n");
            sign = - sign;
        }
        d_check = 0;
        i = -1;
    }
    i++;

    // Yaw correction
    if (a_ref < 6 && a_ref > -6) sp.gamma += 0;
    else {
        gamma_r0 = - gamma_max * (theta /
            (sqrt(1 + pow(ka * theta, 2))));
        sp.gamma += gamma_r0;
        theta = 0;
    }

    // Jump map velocity computation
    for (j = 0; j < m; j++) {

```

```

        w_x += ARTVA_FIFO[j] * sin(j*OMEGA_x);
        w_y += ARTVA_FIFO[j] * sin(j*OMEGA_y);
        if (ARTVA_FIFO[j] != '\0') k++;
    }
    w_x = w_x / k;
    w_y = w_y / k;

    // Flow map velocity computation
    v_x = - k1_x * v_x - k2_x * w_x;
    v_y = - k1_y * v_y - k2_y * w_y;
    v_x = v_max * (v_x / (sqrt(1 + pow(v_x, 2))));
    v_y = v_max * (v_y / (sqrt(1 + pow(v_y, 2))));
    w_x = 0;
    w_y = 0;

    // Position set-point computation in body frame
    H = ((kh * d_ref) / (sqrt(1 + pow(kh * d_ref, 2))));
    p_x = sign * H * v_x;
    p_y = sign * H * v_y;

    // Reference system transformation from body to hearth frame (NED)
    sp.p_rx = p_x * cos(yaw+sp.gamma) +
    p_y * sin(yaw+sp.gamma) + RHO_x * cos(OMEGA_x * t);
    sp.p_ry = - p_x * sin(yaw+sp.gamma) +
    p_y * cos(yaw+sp.gamma) + RHO_y * sin(OMEGA_y * t);
    sp.hesc_mode = 1;
    orb_publish(ORB_ID(sp_data), sp_topic_pub, &sp);
    t++;

    return 0;
}

```





# Bibliography

- [1] L. Marconi, C. Melchiorri, M. Beetz, D. Pangercic, R. Siegwart, S. Leutenegger, R. Carloni, S. Stramigioli, H. Bruyninckx, P. Doherty, A. Kleiner, V. Lippiello, A. Finzi, B. Siciliano, A. Sala, N. Tomatis, “The SHERPA project: smart collaboration between humans and ground-aerial robots for improving rescuing activities in alpine environments”, 10th IEEE International Symposium on Safety Security and Robotics, 2012.
- [2] H. Brugger, B. Durrer, F. Elsensohn, P. Paal, G. Strapazzon, E. Winterberger, K. Zafren, J. Boyd, “Resuscitation of avalanche victims: Evidence-based guidelines of the international commission for mountain emergency medicine (ICAR MED-COM)”, *Resuscitation*, Volume 84, Issue 5 , Pages 539-546, May 2013
- [3] M. Silvagni, A. Tonoli, E. Zenerino, M. Chiaberge (2017), “Multipurpose UAV for search and rescue operations in mountain avalanche events”, *Geomatics, Natural Hazards and Risk*, 8:1, 18-33.
- [4] N. Mimmo, M. Furci, F. Callegati, and Lorenzo Marconi, “A supervisory strategy for quick localization of buried victims by aerial vehicles”, Department of Electrical, Electronic and Information Engineering, University of Bologna.
- [5] K. B. Ariyur, M. Kristic, “Real-Time Optimization by Extremum-Seeking Control”, Wiley-Interscience, A John Wiley & sons, INC., publication.
- [6] Y. Tan, D. Nesic, and I.M.Y.Mareels, “On non-local stability properties of Extremum Seeking Control”, the Department of Electrical & Electronics, the University of Melbourne, Parkview, VIC 3010.

- [7] R. Goebel, R. G. Sanfelice, and A. R. Teel, “Hybrid Dynamical Systems: Modelling, Stability, and Robustness”, Princeton University Press, 2012.
- [8] N. Mimmo and L. Marconi, “Hybrid Extremum Seeking Control for Avalanche Victims Search”, Department of Electrical, Electronic and Information Engineering, University of Bologna.
- [9] Website of PX4: <https://dev.px4.io>
- [10] Website of Sparkfun: <https://learn.sparkfun.com>
- [11] Website of ROS: <http://ros.org>